Global and Planetary Change 168 (2018) 35–53

Contents lists available at ScienceDirect

Global and Planetary Change

journal homepage: www.elsevier.com/locate/gloplacha

Research article

Millennial-scale cyclical environment and climate variability during the Holocene in the western Mediterranean region deduced from a new multi-proxy analysis from the Padul record (Sierra Nevada, Spain)

María J. Ramos-Román[a,*], Gonzalo Jiménez-Moreno[a], Jon Camuera[a], Antonio García-Alix[a,b], R. Scott Anderson[c], Francisco J. Jiménez-Espejo[d], Dirk Sachse[e], Jaime L. Toney[f], José S. Carrión[g], Cole Webster[c], Yurena Yanes[h]

[a] Departamento de Estratigrafía y Paleontología, Universidad de Granada, Spain
[b] Instituto Andaluz de Ciencias de la Tierra (IACT), CSIC-UGR, Armilla, Spain
[c] School of Earth Sciences and Environmental Sustainability, Northern Arizona University, USA
[d] Department of Biogeochemistry, Japan Agency for Marine-Earth Science and Technology (JAMSTEC), Japan
[e] Helmholtz Centre Potsdam, German Research Centre for Geosciences GFZ, Section 5.1 Geomorphology, Organic Surface Geochemistry Lab., Germany
[f] School of Geographical and Earth Sciences, University of Glasgow, UK
[g] Departamento de Biología Vegetal, Facultad de Biología, Universidad de Murcia, Murcia, Spain
[h] Department of Geology, University of Cincinnati, USA

ARTICLE INFO

Keywords:
Holocene
Padul
Wetland
Sierra Nevada
Western Mediterranean
Atmospheric-oceanic dynamics
Wavelet analysis
Arid events

ABSTRACT

A high-resolution multi-proxy approach, integrating pollen, inorganic and organic geochemical and sedimentological analyses, has been carried out on the Holocene section of the Padul sedimentary record in the southern Iberian Peninsula reconstructing vegetation, environment and climate throughout the last ~ 11.6 cal kyr BP in the western Mediterranean. The study of the entire Holocene allows us to determine the significant climate shift that occurred during the middle-to-late Holocene transition. The highest occurrence of deciduous forest in the Padul area from ~ 9.5 to 7.6 cal kyr BP represents the Holocene humidity optimum probably due to enhanced winter precipitation during a phase of highest seasonal anomaly and maximum summer insolation. Locally, insolation maxima induced high evaporation, counterbalancing the effect of relatively high precipitation, and triggered very low water table in Padul and the deposition of peat sediments. A transitional environmental change towards more regional aridity occurred from ~ 7.6 to 4.7 cal kyr BP and then aridification enhanced in the late Holocene most likely related to decreasing summer insolation. This translated into higher water levels and a sedimentary change at ~ 4.7 cal kyr BP in the Padul wetland, probably related to reduced evaporation during summer in response to decreased in seasonality. Millennial-scale variability is superimposed on the Holocene long-term trends. The Mediterranean forest regional climate proxy studied here shows significant cold-arid events around ~ 9.6, 8.5, 7.5, 6.5 and 5.4 cal kyr BP with cyclical periodicities (~1100 and 2100 yr) during the early and middle Holocene. A change is observed in the periodicity of these cold-arid events towards ~1430 yr in the late Holocene, with forest declines around ~ 4.7–4, 2.7 and 1.3 cal kyr BP. The comparison between the Padul-15-05 data with published North Atlantic and Mediterranean paleoclimate records suggests common triggers for the observed climate variability, with the early and middle Holocene forest declines at least partially controlled by external forcing (i.e. solar activity) and the late Holocene variability associated with internal mechanisms (oceanic-atmospheric).

1. Introduction

The western Mediterranean region, located in the subtropical latitude (Alpert et al., 2006), is a sensitive area to detect past climate variability and has been the focus of several previous Holocene studies (e.g., Fletcher et al., 2013; Zielhofer et al., 2017). Present-day climate in this area is characterized by a strong seasonality, principally dominated by dry (hot) summers and wetter (mild) winters (Lionello et al., 2006) and one of the main mechanisms driving climate variations is the North Atlantic Oscillation (NAO) (Hurrell, 1995; Moreno et al., 2005).

* Corresponding author.
E-mail address: mjrr@ugr.es (M.J. Ramos-Román).

https://doi.org/10.1016/j.gloplacha.2018.06.003
Received 20 March 2018; Received in revised form 29 May 2018; Accepted 7 June 2018
Available online 08 June 2018
0921-8181/

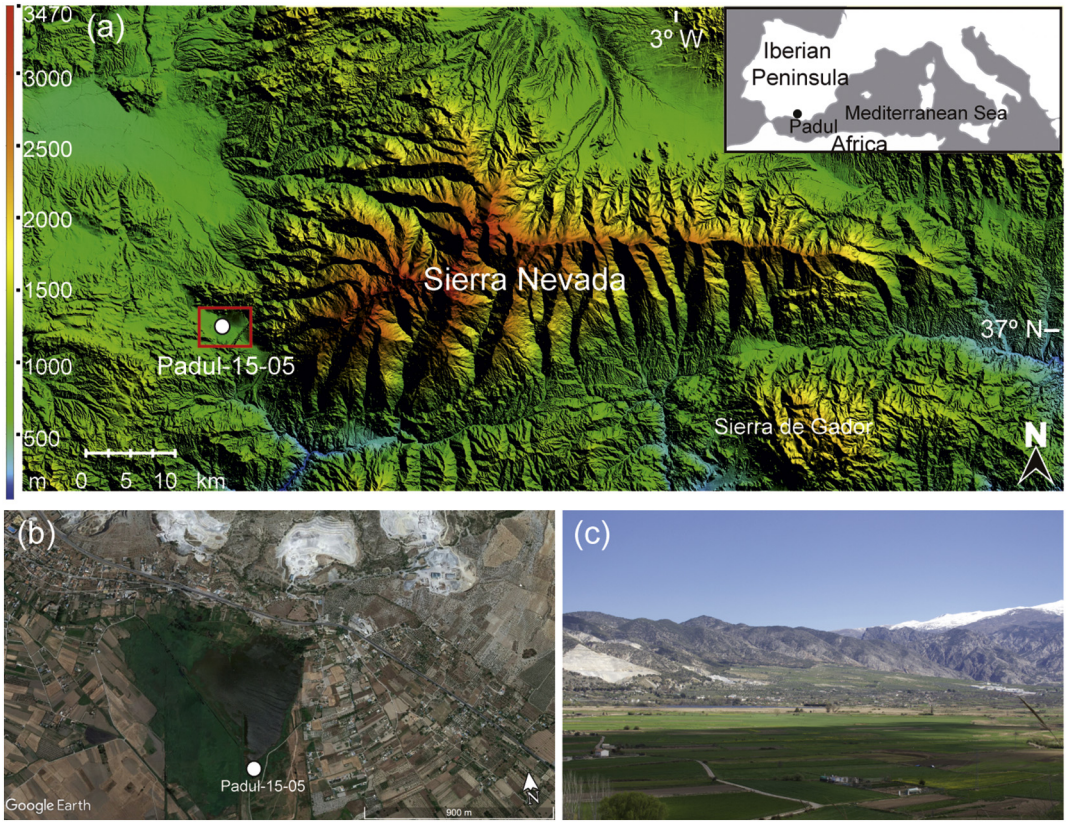

Fig. 1. Location and pictures of Padul wetland. (a) Location of Padul wetland in Sierra Nevada, southern Iberian Peninsula, with an inset showing south western Europe. (b) Padul basin area showing the coring location. (c) Picture of Padul wetland, peat bog and crops area in the Padul basin, and the alluvial fans and Sierra Nevada mountains in the background. Picture from M.J. Ramos-Román. Software use: Above, Sierra Nevada map was performed using the GIS software Global Mapper (http://www.globalmapper.com) and modified with Adobe Illustrator. The inset map (the western Mediterranean region) was created with Adobe Illustrator (https://www. adobe.com/). Below, left, is the Google earth image (http://www.google.com/earth/index.html) of the Padul basin showing the coring locations.

During the Holocene, orbital-scale (i.e. insolation) variations triggered climate changes that in turn produced significant environmental changes worldwide. Paleoclimate records show a Holocene climatic optimum between 9.5 and 7.5 cal kyr BP (Dormoy et al., 2009), characterized in the western Mediterranean area by high temperatures and precipitation, which has been related with high summer insolation (Lamb and van der Kaars, 1995; Fletcher and Sánchez-Goñi, 2008; Anderson et al., 2011). Regional climate models described that the most important climatic transition towards cooler and drier conditions during the Holocene occurred around ~ 6 ka (Huntley and Prentice, 1988; Cheddadi et al., 1997). This shift has also been documented in the western Mediterranean, suggesting the establishment of the current NAO-like system at ~ 6 cal kyr BP (Fletcher et al., 2013). However, other studies differ in the timing of this climate shift indicating a transition phase between 7 and 5.5 cal kyr BP (Jalut et al., 2009). These differences could be related with changes in altitudinal vegetation gradient, geomorphological changes in the study area and/or human perturbance of the landscape (Anderson et al., 2011). According to Roberts et al. (2011), combining different proxies indicative of vegetation and geomorphological changes is a useful tool to discern the timing and the main forcing triggering this mid-Holocene environmental changes.

During the last few decades, a multitude of continental, marine and ice records worldwide have shown millennial-scales climate variability during the Holocene (e.g. Johnsen et al., 1992; Bar-Matthews et al., 2003; Mayewski et al., 2004). Numerous studies have detected this climate variability in the North Atlantic area (i.e., Bond et al., 2001; Debret et al., 2007, 2009), with a prominent ~ 1500 yr cyclicity throughout the Holocene (Bond et al., 2001). However, others studies have demonstrated that Holocene climate variability was not stationary and exhibited variable periodicity at different times-intervals (Debret et al., 2007, 2009). In this respect, high-resolution Mediterranean records have also shown rapid environmental variability related to millennial-scale climate variability (Cacho et al., 2001; Fletcher and Sánchez-Goñi, 2008; Peyron et al., 2013). Previous palynological analyses from the western Mediterranean showed vegetation responses at millennial-scales that seem to co-vary with climate variability from North Atlantic records, demonstrating hemispheric-scale teleconnections during the Holocene (Combourieu-Nebout et al., 2009; Fletcher et al., 2013; Rodrigo-Gámiz et al., 2014a). Other marine and terrestrial studies found centennial and millennial-scale Holocene frequency climatic patterns (Rodrigo-Gámiz et al., 2014a; Ramos-Román et al., 2016; García-Alix et al., 2017). However, there is a lack of non-stationary time-series analysis at millennial-scales from terrestrial records in the western Mediterranean area, which is necessary to understand terrestrial-ocean-atmospheric dynamics and the connections with high-latitude North Atlantic climate records. This is key for learning about past environmental change and climate variability in the western Mediterranean region.

Multi-proxy studies on continental records in southern Iberia and the western Mediterranean that could help understanding this environmental variability during the Holocene are rare. In order to improve our knowledge about this subject, we present a high-resolution multidisciplinary analysis integrating sedimentation, geochemistry, vegetation, and climate change and variability during the Holocene (from ~11.6 cal kyr BP to Present) from the Padul-15-05 wetland record. Previous sedimentary records and paleoecological studies have been carried out on the Padul archive, detecting climate variability from the Pleistocene to the middle Holocene (Florschütz et al., 1971; Pons and Reille, 1988; Ortiz et al., 2004). Nevertheless, a high-

resolution multi-proxy analysis on the same sediment samples has never been performed at this site for the entire Holocene epoch. Recently, a multi-proxy analysis [studying pollen, spores, magnetic susceptibility (MS), total organic carbon (TOC) and X-ray fluorescence (XRF)] has been done focusing on the late Holocene part of the Padul-15-05 record. That study shows an aridification trend since ~ 4.7 cal kyr BP and enhanced human influence on the environments in the area since the last 1.5 cal kyr BP (Ramos-Román et al., 2018), renewing the interest to carry out a more complete study for the entire Holocene. The present study uses high-resolution radiocarbon dating, inorganic and organic geochemistry (biomarkers and bulk sediment), pollen, lithology and macrofossil analyses to reconstruct the Padul area paleoenvironmental evolution and millennial-scale vegetation and climate fluctuations in the western Mediterranean region over the last 11,600 years. This research seeks two main goals: 1) understanding regional vegetation changes and local environmental evolution and making climate interpretations during the early, middle and late Holocene, specifically focusing on the transitions, and 2) comparing millennial-scale vegetation and water-level oscillations (regional and local signal) with global climatic events.

1.1. Location and environmental setting

The Padul basin is an endorheic area at around 725 m of elevation at the foothill of the southwestern Sierra Nevada in Andalusia, southern Spain (Fig. 1). Today's climate in the Padul area is characterized by a mean annual temperature of 14.4 °C and a mean annual precipitation of 445 mm, and by hot and dry summers (mean temperature of 22.8 °C and precipitation of 25 mm) and mild and wetter winters (mean temperature of 8 °C and precipitation of 140 mm) (http://agroclimap.aemet.es/). The Sierra Nevada mountain range shows strong thermal and precipitation differences due to the altitudinal gradient (from ~700 to > 3400 m), which controls plant taxa distribution in different bioclimatic vegetation belts due to the variability in temperature and precipitation (Valle Tendero, 2004). According to this climatophilous series classification (Table 1), the Padul basin is situated in the Mesomediterranean vegetation belt (from ~ 600 to 1400 m of elevation), which is largely defined by the dominance of *Quercus rotundifolia* (evergreen *Quercus* pollen morphotype) and, to a lesser extent, *Q. faginea* (deciduous *Quercus* pollen morphotype), which is normally accompanied by *Pistacia terebinthus*. *Q. coccifera* (evergreen *Quercus* pollen morphotype) also occur in crests and very sunny rocky outcrops.

Sedimentation in the Padul basin results from (1) allochthonous detritic material coming for the surrounding mountains, principally from Sierra Nevada, which is characterized at higher elevations by Paleozoic siliceous metamorphic rocks (mostly mica-schists and quartzites) from the Nevado-Filabride complex and, at lower elevations and acting as bedrock, by Triassic dolomites, limestones and phyllites from the Alpujárride Complex (Sanz de Galdeano et al., 1998), (2) autochthonous organic material coming from plants growing in the wetland area of the basin itself and (3) biogenic carbonates from charophytes, ostracods and gastropod shells, prominent organisms that lived in the lake. The water contribution to the Padul wetland primarily comes from groundwater input and, to a lesser degree, from rainfall. Groundwater comes from different aquifers: the Triassic carbonate aquifers to the north and south edge of the basin, the out-flow of the Granada Basin to the west and the conglomerate aquifer to the east (Castillo Martín et al., 1984; Ortiz et al., 2004). The main water output is trough evaporation and evapotranspiration and more recently also by water wells and by canals (locally called “madres”) (Castillo Martín et al., 1984). The canals were built around the end of the XVIII century with the goal of draining the basin water to the Dúrcal river to the southeast for cultivation purposes (Villegas Molina, 1967). In the early 2000s the Padul wetland was placed under environmental protection and the peat mine stopped pumping water out of the basin and the Padul lake increased its size considerably.

The Padul-15-05 drilling site is located around 50 m south of the present-day Padul lake-shore area. The edge of the lake area is at present principally dominated by the grass *Phragmites australis*. The lake environment is also characterized by emerged and submerged macrophytes communities dominated by *Chara vulgaris*, *Myriophyllum spicatum*, *Potamogeton pectinatus*, *Potamogetum coloratus*, *Typha dominguensis*, *Apium nodiflorum*, *Juncus subnodulosus*, *Carex hispida*, *Juncus bufonius* and *Ranunculus muricatus* among others (Pérez Raya and López Nieto, 1991). *Populus alba*, *Populus nigra*, *Ulmus minor* and several species of *Salix* and *Tamarix* grow on the northern lake shore (Ramos-Román et al., 2018).

2. Methodology

2.1. Padul site core drilling

The Padul-15-05 sediment core (37°00′39.77″N; 3°36′14.06″W) with a length of 42.64 m, was collected in 2015 from the Padul lake shore (Fig. 1). The core was taken with a Rolatec RL-48-L drilling machine equipped with a hydraulic piston corer from the Scientific Instrumentation Center of the University of Granada (CIC-UGR). The sediment core was wrapped in film, put in core boxes, transported and stored in a dark cool room at + 4 °C at the University of Granada. In this study, we focus on the uppermost ~ 3.67 m from the 42.6-m-long Padul-15-05 core.

2.2. Chronology and sedimentation rates

The age model for the uppermost ~ 3.27 m is based on fourteen AMS radiocarbon dates previously shown in Ramos-Román et al. (2018). Six more radiocarbon samples have been analyzed in the lower part of the study record in order to improve the chronology of older sediments. Three of these samples were rejected, because one plant sample was too young and two gastropod shell samples provided old dates due to the reservoir effect. As a result, the sedimentary record chronology from ~ 4.24 m to 0.21 m depth was constrained using a total of seventeen AMS radiocarbon dates (Table 2). The age model was built using the R-code package ‘Clam 2.2’ employing the calibration curve IntCal 13 (Reimer et al., 2013), a 95% confident range, a smooth spline (type 4) with a 0.20 smoothing value and 1000 iterations (Fig. 2). The chronology of the uppermost 21 cm of the record was built using a linear interpolation between the last radiocarbon date and the top of the record, which was assigned the age when coring (2015 CE).

In this paper we followed the three principal subdivisions for the Holocene defined by Walker et al., 2012. They proposed an Early-Middle Holocene boundary at 8.2 cal kyr BP and Middle-Late Holocene

Table 1
Modern vegetation belts from Sierra Nevada (El Aallali et al., 1998; Valle, 2003).

Vegetation belt	Elevation (m)	Main taxa
Crioromediterranean	> 2800	Tundra vegetation including members of Poaceae, Asteraceae, Brassicaceae, Gentianaceae, Scrophulariaceae and Plantaginaceae.
Oromediterranean	1900–2800	*Pinus sylvestris*, *P. nigra* and *Juniperus* spp. and other shrubs such as species of Fabaceae, Cistaceae and Brassicaceae.
Supramediterranean	1400–1900	*Quercus pyrenaica*, *Q. faginea* and *Q. rotundifolia* and *Acer opalus* ssp. *granatense* and other trees and shrubs, with some species of Fabaceae, Thymelaeaceae, Cistaceae and *Artemisia* sp.
Mesomediterranean	600–1400	*Quercus rotundifolia*, some shrubs, herbs and plants as *Juniperus* sp., and some species of Fabaceae, Cistaceae and Liliaceae

Table 2
Age data for Padul-15-05 record. All ages were calibrated using R-code package 'clam 2.2' employing the calibration curve IntelCal 13 (Reimer et al., 2013) at 95% of confident range. Note that the age data for the uppermost ~ 3.27 m were previously shown (Ramos-Román et al., 2018).

Laboratory number[a]	Core	Material	Depth (cm)	Age (^{14}C yr BP ± 1σ)	Calibrated age (cal yr BP) 95% confidence interval	Median age (cal yr BP)
Reference ages			0	2015 CE	−65	−65
D-AMS 008531	Padul-13-01	Plant remains	21.67	103 ± 24	23–264	125
Poz-77,568	Padul-15-05	Org. bulk sed.	38.46	1205 ± 30	1014–1239	1130
BETA-437233	Padul-15-05	Plant remains	46.04	2480 ± 30	2385–2722	2575
Poz-77,569	Padul-15-05	Org. bulk sed.	48.21	2255 ± 30	2158–2344	2250
BETA-415830	Padul-15-05	[b]Shell	71.36	3910 ± 30	4248–4421	4345
BETA- 437234	Padul-15-05	Plant remains	76.34	3550 ± 30	3722–3956	3840
BETA-415831	Padul-15-05	Org. bulk sed.	92.94	3960 ± 30	4297–4519	4430
Poz-74,344	Padul-15-05	Plant remains	122.96	4295 ± 35	4827–4959	4870
BETA-415832	Padul-15-05	Plant remains	150.04	5050 ± 30	5728–5900	5815
Poz-77,571	Padul-15-05	Plant remains	186.08	5530 ± 40	6281–6402	6340
Poz-74,345	Padul-15-05	Plant remains	199.33	6080 ± 40	6797–7154	6935
BETA-415833	Padul-15-05	Org. bulk sed.	217.36	6270 ± 30	7162–7262	7210
Poz-77,572	Padul-15-05	Org. bulk sed.	238.68	7080 ± 50	7797–7999	7910
Poz-74,347	Padul-15-05	Plant remains	277.24	8290 ± 40	9138–9426	9295
BETA-415834	Padul-15-05	Plant remains	327.29	8960 ± 30	9932–10,221	10,105
Poz-77,573	Padul-15-05	Plant remains	340.04	9420 ± 50	10,514–10,766	10,640
Poz-74,348	Padul-15-05	[b] Plant ramains	375.62	9120 ± 50	10,199–10,412	10,305
Poz-79,815	Padul-15-05	Org. Bulk sed.	377.83	10,310 ± 50	11,847–12,388	12,145
Poz-79,817	Padul-15-05	[b]Shell	411.02	13,910 ± 60	16,588–17,088	16,840
Poz-79,818	Padul-15-05	[b]Shell	414.89	14,130 ± 50	17,001–17,419	17,210
Poz-77,574	Padul-15-05	Org. Bulk sed.	423.65	13,580 ± 80	16,113–16,654	16,385

[a] Sample number assigned at radiocarbon laboratory.
[b] Rejected data.

at 4.2 cal kyr BP.

2.3. Lithology and magnetic susceptibility (MS)

The Padul-15-05 core was split longitudinally and was described in the laboratory with respect to lithology and colour (Fig. 3). High-resolution continue scanning images were taken with an Avaatech core scanner at the University of Barcelona (UB). MS was measured with a Bartington MS3 operating with a MS2E sensor. MS measurements (in SI units) were obtained directly from the core surface every 0.5 cm (Fig. 3). Lithological description and MS data of the same record of the uppermost 1.15 m of the record were previously described in Ramos-Román et al. (2018).

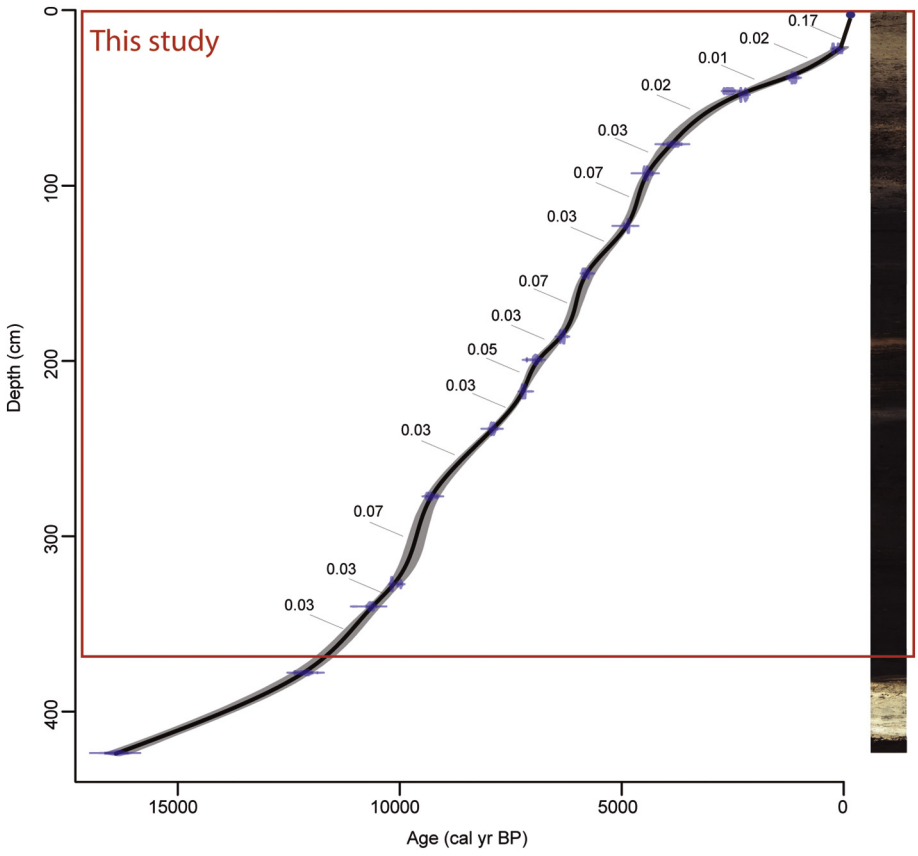

Fig. 2. Picture of the Padul-15-05 sediment core (images were taken with an Avaatech core scanner at the University of Barcelona) with the age-depth model showing the part of the record that was studied here (red rectangle) corresponding with the last ~11.600 years, based on a previous age-depth model (Ramos-Román et al., 2018). The sediment accumulation rates (SAR; unit = cm/yr) between radiocarbon dates are marked. See the body of the text for the explanation of the age reconstructions. (For interpretation of the references to colour in this figure legend, the reader is referred to the web version of this article.)

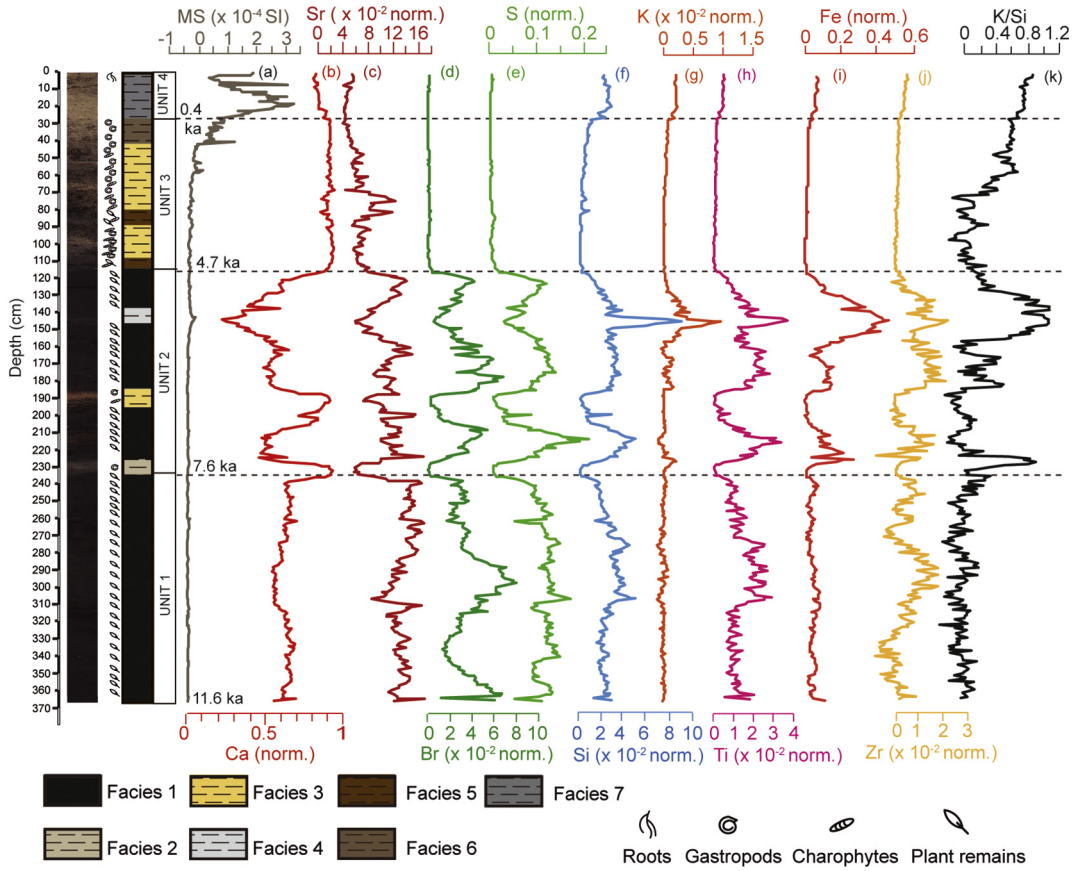

Fig. 3. Inorganic geochemistry results for the ~3.67 m of the upperpart from Padul 15–05 record. Picture of the Padul-15-05 record, facies interpretations with paleontology, magnetic susceptibility (MS) and X-ray fluorescence (XRF). XRF elements (Ca, Sr, Br, S, Si, K, Ti, Fe, Zr) are represents as counts per second normalized to the total counts (norm.). (a) MS in SI, (b) Calcium normalized (Ca norm.) (c) Strontium normalized (Sr norm.) (d) Bromine normalized (Br norm.) (e) Sulfur normalized (S norm.) (f) Silica normalized (Si norm.), (g) Potassium normalized (K norm.), (h) Titanium normalized (Ti norm.), (i) Iron normalized (Fe norm.), (j) Zirconium normalized (Zr norm.), (k) K/Si ratio. Note that uppermost ~ 1.15 m inorganic geochemistry results of the record were previously shown in Ramos-Román et al. (2018).

2.4. Inorganic geochemistry

High-resolution XRF was applied continuously throughout the core surface, taking measurements of elemental geochemical composition. An Avaatech X-Ray fluorescence (XRF) core scanner® located at the UB was used. Chemical elements were measured in the XRF core scanner at 10 mm of spatial resolution, using 10 s count time, 10 kV X-ray voltage and an X-ray current of 650 μA for lighter elements and 35 s count time, 30 kV X-ray voltage, X-ray current of 1700 μA for heavier elements. Thirty-three chemical elements were measured but only the most representative with a significant number of counts were considered (Si, K, Ca, Ti, Fe, Zr, Br, S and Sr). Results for each element are expressed as intensities in counts per second (cps) and normalized for the total sum in cps in every measure (Fig. 4), being the upper part of the record (from 1.15 m to the top) previously shown in Ramos-Román et al. (2018).

2.5. Organic geochemistry

Several organic geochemical proxies have been studied from bulk sediment samples throughout the record: total organic carbon (TOC), atomic Carbon-Nitrogen ratio (C/N) and atomic Hydrogen-Carbon ratio (H/C). In addition, several indices of leaf wax biomarkers (*n*-alkanes) were calculated: the average chain length (ACL), the carbon preference index (CPI) and the portion of aquatic (Paq). In addition, three new indices have been calculated based on the relative abundance of odd carbon number from nC_{17} to nC_{33} alkanes, except for nC_{27} alkanes (See Section 3.2.2 for justification of new indices).

Samples for elemental analyses in bulk sediment were analyzed every 2 or 3 cm throughout the Padul-15-05 record, with a total of 206 samples analyzed. Samples were decalcified with 1:1 HCl to eliminate the carbonate fraction. Carbon, nitrogen and hydrogen content of the decalcified samples were measured in an Elemental Analyzer Thermo Scientific Flash 2000 model at the CIC-UGR. Percentage of TOC (note that TOC of the uppermost 1.15 m of the record was previously described; Ramos-Román et al., 2018), total nitrogen (TN) and total hydrogen (TH) per gram of sediment was calculated from the percentage of organic carbon, nitrogen and hydrogen yielded by the elemental analyzer, and recalculated by the weight of the sample prior to decalcification. The atomic C/N and H/C ratio was calculated from the carbon, nitrogen and hydrogen measurements (Fig. 4).

Biomarkers from the Padul-15-05 record were extracted every 5 cm from sedimentary record, with a total of 68 samples analyzed. Furthermore, thirty-one modern plant leaves/algae and bryophyte samples were taken from the surroundings of the Padul basin and analyzed for biomarkers. The total lipid extraction (TLE) from the freeze-dried samples was obtained using an accelerate solvent extractor (ASE) Thermo DIONEX 350, with a dichloromethane:methanol (9:1). Plant biomarkers were extracted manually using dichloromethane:methanol (9:1) by means of sonication and low temperature (38 °C). The TLE from plants and sediments was separated into three different fractions using a silica gel column. Before the separation

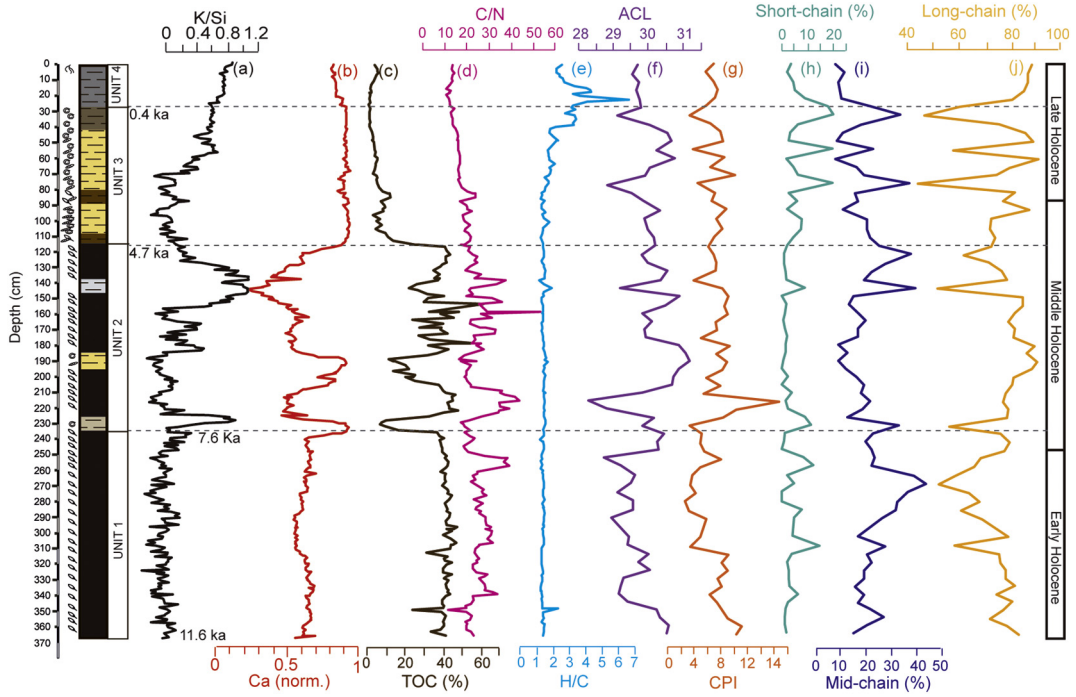

Fig. 4. Organic geochemistry results for the ~3.67 m of the upperpart (Holocene part) from Padul-15-05 record and comparison with inorganic index calculated from the PCA analysis performed to XRF elements in the same record. (a) K/Si ratio, (b) Ca (norm.), (c) Total organic carbon percentage (TOC %), (d) Carbon-Nitrogen ratio (C/N), (e) Hydrogen-Carbon ratio (H/C), (f) Average chain length (ACL), (g) Carbon preference index (CPI), (h) Short-chain (%), (i) Mid-chain (%), (j) Long-chain (%). Note that the uppermost ~ 1.15 m TOC values were previously shown (Ramos-Román et al., 2018).

three internal standards were added to the TLE (5α-androstane, 5β-androstan-17-one and 5α-androstan-3β-ol) in order to assess the biomarker extraction as well as to quantify them. Compounds of the aliphatic fraction (*n*-alkanes) were recovered in the first fraction eluted with Hexane. The *n*-alkanes were identified and quantified using a Gas Chromatography flame detection and mass spectrometry (GC-FID and GC–MS) by means of an Agilent 5975C MSD by comparison to an external *n*-alkane standard mixture from nC_{10} to nC_{40}.

2.6. Pollen

Samples for pollen analysis (1–3 cm3) were taken with a resolution between 1 and 5 cm throughout the core. A total of 73 samples between 1.15 and 3.67 m have been analyzed in this study and were summed to the previous 103 pollen samples analyzed between 0 and 1.15 m (Ramos-Román et al., 2018), with a mean pollen resolution around 65 yr (~ 95 yr between 11.6 and 4.7 cal kyr BP and ~ 50 yr for the last 4700 years). Pollen extraction methods followed a modified Faegri and Iversen (1989) methodology. Processing included the addition of *Lycopodium* spores for calculation of pollen concentration. Sediment was treated with 10% NaOH, 10% HCl, 10% HF and the residue was sieved at 250 μm before an acetolysis solution. Counting was performed using a transmitted light microscope at 400 magnifications to an average pollen count of around 250 terrestrial pollen grains. Fossil pollen was identified using published keys (Beug, 2004) and modern reference collections at the UGR. Pollen counts were transformed to pollen percentages based on the terrestrial pollen sum, excluding aquatics. Non-pollen palynomorphs (NPP) include algal spores. The NPP percentages were also calculated and represented with respect to the terrestrial pollen sum. Several pollen and NPP taxa were grouped according to present-day ecological data in Mediterranean forest, xerophytes and algae (Fig. 5). The Mediterranean forest taxa include *Quercus* total, *Olea*, *Phillyrea*, *Pistacia* and Cistaceae. The Xerophyte group includes *Artemisia*, *Ephedra*, and Amaranthaceae. The Algae group is composed of *Botryococcus*, *Zygnema* type, *Mougeotia* and *Pediastrum*. Zonation was obtained witha cluster analysis using four representative pollen taxa Mediterranean forest, *Pinus* total, Ericaceae and *Artemisia* (Grimm, 1987; Fig. 5).

2.7. Statistical analysis

Statistical treatment was performed using the *PAST 3.12* software (Hammer et al., 2001). Principal component analysis (PCA) was conducted on different geochemical elements (XRF data) to clarify the lithological elemental composition of the core (Supplementary; Fig. S1). Prior to the PCA analysis, we pretreated the data normalizing the element counts by subtracting the mean and dividing by the standard deviation (Davis and Sampson, 1986). As data spacing was different in all the study proxies, the data were also resampled to the average value of 80-yr (linear interpolation) to obtained equally spaced time series. Posteriorly, a Pearson correlation was made to different organic/inorganic geochemistry and pollen proxies to find affinities between the different proxies.

In this study, spectral analysis was accomplished on the Mediterranean forest pollen taxa time series, to identify regional millennial-scale periodicities in the Padul-15-05 record. We used REDFIT software (Schulz and Mudelsee, 2002) on the unevenly spaced pollen time series in order to identify cyclical changes. In addition, we carried out a Wavelet transform analysis by the PAST software (Torrence and Compo, 1998) with the goal of identifying non-stationary cyclical variability in the regional vegetation evolution, the pollen was previously detrended and resampled at 80-yr age increments. In this study, a Morlet wavelet was chosen, the significant level (plotted as contour) corresponded to a *p*-value = .05, and a white-noise model was implemented.

2.8. Correlations for the environment reconstruction

Linear r (Pearson) correlation analyses between the obtained local proxy dataset (MS, Ca, S, Br, Sr, K/Si ratio, C/N ratio, H/C ratio, TOC,

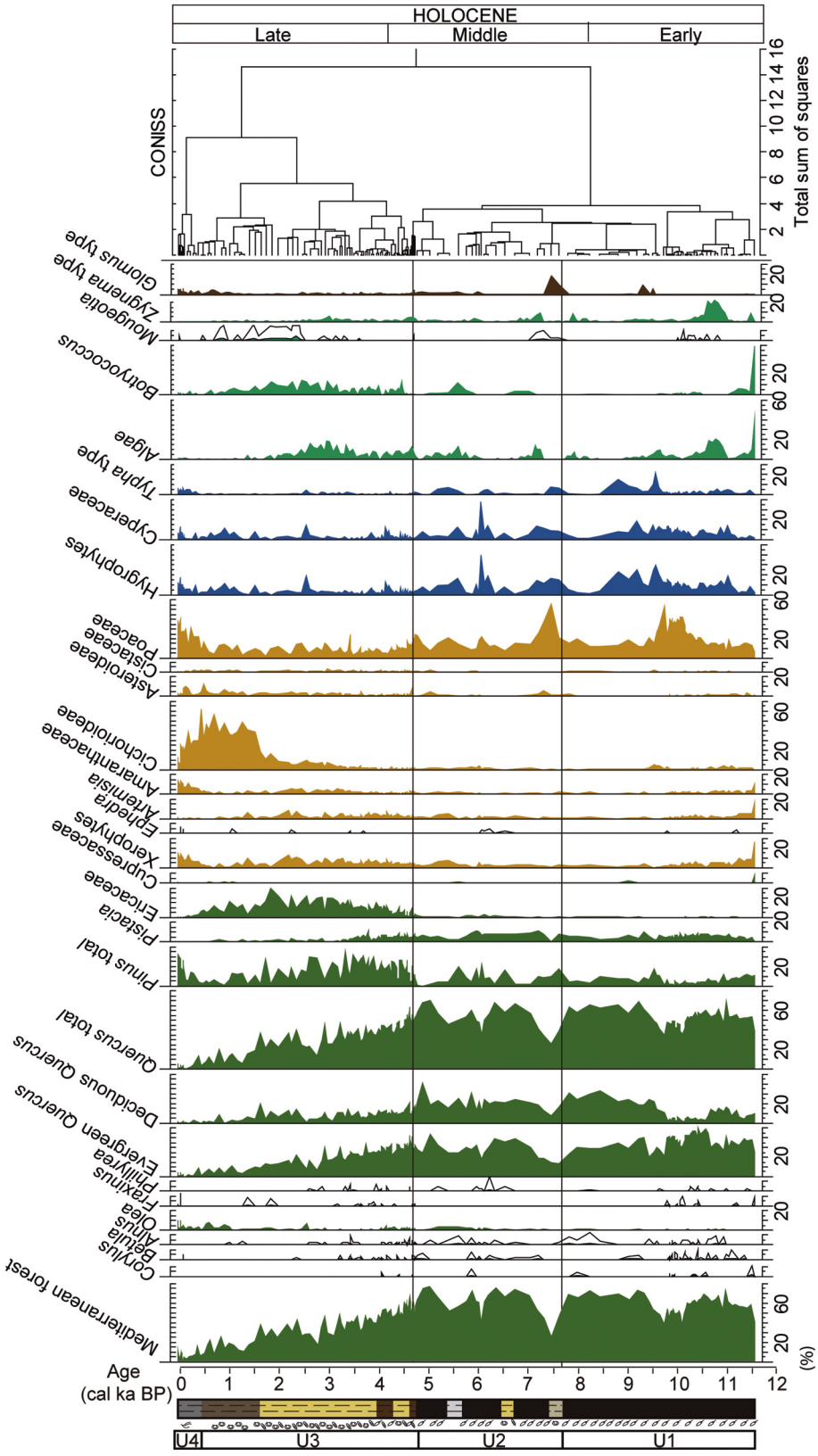

Fig. 5. Percentages of selected pollen taxa and non-pollen palynomorphs (NPPs) from the Holocene part of Padul-15-05 record, represented with respect to terrestrial pollen sum. Silhouettes show 7-time exaggerations of pollen percentages. Tree and shrubs are showing in green, herbs and grasses in yellow, aquatics in dark blue, algae in blue and fungi in brown. The Mediterranean forest taxa is composed of *Quercus* total, *Olea*, *Phillyrea* and *Pistacia*. The xerophyte group includes *Artemisia*, *Ephedra*, and Amaranthaceae. The hygrophytes group is composed by Cyperaceae and *Typha* type. Algae group is formed by *Zygema* type, *Botryococcus*, *Mougeotia* and *Pediastrum*. U: Unit. Note that uppermost ~ 1.15 m pollen and NPPs results of the record were previously depicted (Ramos-Román et al., 2018). (For interpretation of the references to colour in this figure legend, the reader is referred to the web version of this article.)

short-chain, mid-chain and long-chain abundances, Poaceae, Algae and Hygrophytes) are shown in Table 4. These analyses were performed to identify the associations between proxies and to understand environmental change in the Padul area. This analysis assisted us in identifying (a) different proxies characteristic of organic-rich sediments, primarily that peatland environment under very shallow lake conditions (higher TOC, C/N ratio, S, Br, Sr and mid-chain abundance) and (b) a second group of proxies characteristic of deeper shallow water environments depicted by the increase in endogenic carbonates and more influenced by terrestrial-clays input (higher Ca, K/Si, MS, Algae).

3. Results and proxy interpretation

3.1. Chronology and sedimentary rates

The age-model of the studied Padul-15-05 core (Fig. 2) is constrained by 17 AMS ^{14}C radiocarbon dates from the top 4.24 m of the record (Table 2). In this work, we studied the uppermost ~ 3.67 m that continuously cover the last ~ 11.6 cal kyr BP. This interval is chronologically constrained by 16 AMS radiocarbon dates. Fifteen distinct sediment accumulation rates (SAR) intervals are differentiated between 3.67 m and the top of the record (Fig. 2).

3.2. Lithology, inorganic and organic geochemistry

3.2.1. Lithology and inorganic geochemistry

Inorganic geochemistry informs us about variations in the lithology and the local depositional environment. Variations in these proxies could also be useful for estimating water level fluctuations in the wetland environment. Sediments bearing aquatic fossil remains (i.e. gastropods and charophytes) as well as beingrich in carbonates have previously been related to shallow water lakes (Riera et al., 2004). Lower water levels, more subjected to be occupied by wetland vegetation, and ephemeral lakes are characterized by the increase in organics and clastic input and more influenced by terrestrial-fluvial deposition (Martín-Puertas et al., 2008). Magnetic susceptibility (MS) measures the propensity of the sediments to bring a magnetic charge (Snowball and Sandgren, 2001).

Framboidal pyrite (FeS_2) and barite ($BaSO_4$) with Sr have been found covering exceptionally preserved mammals remains from 40 to 30 ka at the Padul Peat bog (García-Alix et al., 2012) pointing towards a peat-bog environment with enhanced anoxic conditions. The presence of pyrite and organic-sulfur compounds is common in peat bogs (Wieder and Lang, 1988; Feijtel et al., 1989; Chapman, 2001) and other organic rich sediments under anoxic conditions (López-Buendía et al., 2007). Increasing values of organic carbon and bromine have been related with higher organic matter deposition generated in high productivity environments (Kalugin et al., 2007). In marine records, Br XRF scanning counts can be used to estimates sedimentary total organic carbon (Ziegler et al., 2008).

A visual lithological inspection was made for the upper ~ 3.67 m of the Padul-15-05 sediment core and was compared with the elemental geochemical composition (XRF) and the MS data (Fig. 3). For the geochemical elements, we conducted a PCA to summarize and better understand the correlation between the visual lithological features and the geochemical signal of the sediments (Supplementary Fig. S1 and Table S1). The PCA in the studied sedimentary sequence identifies three main groups of sediments consisting of clays with variable content in (1) carbonates of endogenic formation with high values of Ca, related with the occurrence of shells and charophyte remains, (2) siliciclastics (Si, K, Ti, Fe, Zr) and (3) vegetal organics (related with S and Br) probably associated with reducing environment under anoxic conditions showing high values of S, Sr and Br. The K/Si ratio was calculated to differentiate the clays input into the basin. The K/Si ratio is based on the fact that clay fraction is enriched in phyllosilicates (illite, muscovite), whereas the coarser particles that are mainly quartz, dolomite and schists. This correlation between K and clay content has been observed in other lacustrine systems (e.g. Lake Enol, Iberian Peninsula) and associated with an increase in detrital input (Moreno et al., 2011). Four different lithological units were identified (Fig. 3). Units 1 and 2 are principally made up of peat sediments and Unit 3 and 4 by clays with variable carbonates (Fig. 3). Unit 1 (SAR ~ 0.04 cm/yr), from the bottom (3.67 m; ~ 11.6 cal kyr BP) to around 2.31 m (~ 7.6 cal kyr BP), is characterized by *facies* 1 - dark organic peat – high S, Sr and Br values. Unit 2 (SAR ~ 0.05 cm/yr), from 2.31 to 1.15 m (~ 7.6 to 4.7 cal kyr BP), is also generally characterized by *facies* 1 but with the intercalation of three other different *facies*; *facies* 2 from 2.31 to 2.21 m (~ 7.6 to 7.3 cal kyr BP) depicted by grey clays with gastropod remains (featured by the increase in Ca and K/Si ratio), *facies* 3 from 1.95 to 1.85 m (~ 6.6 to 6.4 cal kyr BP) made up of brown clays with the occurrence of gastropods and charophytes (showing a decrease in S, Br and Sr and higher values of Ca) and *facies 4* around 1.46 to 1.40 m (~ 5.7 to 5.4 cal kyr BP) characterized by grey clays (related with the increase in siliciclastic material and clays input). Units 3 (SAR ~ 0.03 cm/yr) and 4 (SAR ~ 0.13 cm/yr) correspond with the uppermost 1.15 m (4.7 cal kyr BP) of the record were previously described in Ramos-Román et al. (2018) as clays with high Ca values and showing an increasing trend in K/Si ratio to the top of the record.

3.2.2. Organic geochemistry

Variations in TOC, C/N and H/C ratios reflect changes in paleoenvironmental dynamics in bogs and lakes (Meyers and Lallier-Vergès, 1999; Ortiz et al., 2010; García-Alix et al., 2017). TOC concentration is the principal indicator of organic matter content in sediments. Typical organic matter contains 50% of carbon so the concentration of organic matter in sediments is twice the TOC (Meyers and Lallier-Vergès, 1999). C/N ratio informs about the proportion of algae and terrestrial vascular plant organic matter in the sediments (Meyers, 1994). Fresh organic matter from algae exhibits molar C/N values that are between 4 and 10, whereas cellulose-rich terrestrial plants show values above 20 and greater (Meyers, 1994). H/C values are a good proxy for the source of the organic matter in sediments, as algal/bacterial/amorphous remains are richer in hydrogen than herbaceous and woody plant material, with values over 1.7 indicative of algal/amorphous organisms. In addition, lower values of H/C (< 0.8) could also be indicative of organic matter transport or diagenesis after deposition (Talbot, 1988; Talbot and Livingstone, 1989).

N-alkane biomarker abundance and distribution can provide information about different biological sources of organic matter that accumulated in bog and lake sediments (Meyers and Lallier-Vergès, 1999; Ficken et al., 2000; Sachse et al., 2006). Several of these sources are characterized by distinct predominant *n*-alkane chain-lengths that have been identified according to the biological sources to the sediments: (1) In general, *n*-alkanes with 17 or 19 carbon atoms (nC_{17} or nC_{19}) are found predominantly in algae (Gelpi et al., 1970; Cranwell, 1984) and in photosynthetic bacteria (Cranwell et al., 1987), (2) nC_{21}, nC_{23} and nC_{25} are associated with submerged and floating aquatic plants (Cranwell, 1984; Ficken et al., 2000), while (3) *n*-alkane distribution with predominant > nC_{27}, nC_{29}, nC_{31} represents higher terrestrial plant input (Cranwell et al., 1987) as well as emergent macrophytes (e.g. *Juncus* sp., *Typha* sp. or *Phragmites australis*) (Cranwell, 1984; Ogura et al., 1990; Ficken et al., 2000). CPI (illustrating the relative abundance of odd vs. even carbon chain lengths) is a proxy for preservation of organic matter in the sediments, with values lower than 2 indicating diagenetic alteration or algal/bacterial influence and, higher than 2 (see Bush and McInerney, 2013 review) indicating terrestrial influence and thermal immaturity of the source rock. Ficken et al. (2000) formulated the Paq (proportion of aquatics) to discern the origin of the organic inputs in the sediments, giving average values for present-day plants of < 0.1 for terrestrial plants, 0.1–0.4 for emerged aquatics and 0.4–1 for submerged/floating aquatic species.

García-Alix et al. (2017), however, showed that the interpretation of these *n*-alkane chain length indices cannot be generalized, and the modern *n*-alkanes distribution of the vegetation in the study site should be well understood prior to paleoenvironmental interpretations from core records. Accordingly, to better constrain the origin of the organic input in the Padul-15-05 record, we analyzed *n*-alkanes from present day terrestrial and aquatic plants as well as algae/bryophyte in the Padul basin area (Supplementary information; Figs. S2 and S3). Our results show that the predominant *n*-alkanes in the samples are nC_{27}, nC_{29} and nC_{31}. There is also a strong odd-over-even carbon number predominance (CPI values higher than 2). This basin is currently dominated by wetland plants, such as *Phragmites australis* with

Table 3
Summary of the *n*-alkane indices from the studied plant, algae and moss samples from the surroundings of the present-day Padul peatland (For more information see in the Supplementary Fig. S2 and S3).

Samples	n-alkane indices					
	Paq	ACL	CPI	Short-chain (%)	Mid-chain (%)	Long-chain (%)
Algae-Bryophyte	0.32 ± 0.21	27.97 ± 0.74	9.52 ± 7.69	13.02 ± 21.07	35.26 ± 19.82	51.71 ± 33.84
Aquatics plants	0.29 ± 0.34	28.78 ± 1.86	11.60 ± 7.35	1.33 ± 4.40	28.36 ± 32.44	70.31 ± 34.64
Terrestrial	0.16 ± 0.16	28.23 ± 0.74	20.64 ± 10.84	–	17.44 ± 19.34	82.56 ± 19.34

predominant carbon chain between C_{27} and C_{29} *n*-alkane. The Paq for present-day plants average values of 0.16 ± 0.16 for terrestrial plants, 0.29 ± 0.34 for aquatic plants and 0.32 ± 0.21 for algae-bryophyte. ACL average values were around 28.23 ± 0.74 for emerged-terrestrial plants, 28.78 ± 1.86 for aquatic plants and 27.97 ± 0.74 for algae-bryophyte (Table 3; Supplementary Fig. S3). These results led us to the need to create three new *n*-alkane indices with the goal of characterizing the source of organic matter in our sediment samples from the Padul-15-05 record, taking in consideration the relative abundances of the odd carbon chains except for nC_{27} (due to higher values in all the plant/algae samples): (1) Short-chain (%), where higher values are typical from algae or bacterial, (2) Mid-chain (%), where higher values are typical of aquatic plants, and (3) Long-chain (%), where higher values are obtained when the source is vascular emerged aquatic or terrestrial plants (Table 3).

1. Short-chain: $[C_{17}\ -C_{19}] = [(C_{17} + C_{19})/(C_{17} + C_{19} + C_{21} + C_{23} + C_{25} + C_{29} + C_{31} + C_{33})] \times 100$
2. Middle-chain: $[C_{21}\text{-}C_{23}\text{-}C_{25}] = [(C_{21} + C_{23} + C_{25})/(C_{17} + C_{19} + C_{21} + C_{23} + C_{25} + C_{29} + C_{31} + C_{33})] \times 100$
3. Long-chain: $[C_{29}\text{-}C_{31}\text{-}C_{33}] = [(C_{29} + C_{31} + C_{33})/(C_{17} + C_{19} + C_{21} + C_{23} + C_{25} + C_{29} + C_{31} + C_{33})] \times 100$

The results for the organic geochemistry (TOC, C/N ratio, H/C ratio and *n*-alkane indices) from the Padul-15-05 record are illustrated in Fig. 4. TOC values range from 0.8 to 61%, with an average value of 27.5%. Highest TOC values are registered during the deposition of sedimentary Unit 1 averaging values of 41%, associated with the peatland environment and higher values of anoxic/reducing proxies (showing higher correlation with S, Br; Table 4). Higher TOC variability occurred during Unit 2. The transition between Unit 1 and 2 is marked by a TOC decrease with values around 14% at ~ 7.6 cal kyr BP. Other decreases occurred between 2 and 1.89 m (~ 6.9 to 6.4 cal kyr BP) and between 1.48 and 1.39 m (~ 5.7 to 5.4 cal kyr BP), reaching values around 20 and 30%, respectively. The transition between Unit 2 and 3 (~ 4.7 cal kyr BP/~ 1.13 m) is marked by a significant decline to values below 15%. The lowest TOC values are recorded during Units 3 and 4 with average values around 4.6%. Atomic C/N ratios were higher during the lithological Units 1 and 2 and ranged between 53 and 11, with an average value of 26. A decrease in C/N occurred during the transition from Units 2 to 3 down to average values of 17. The lowest values occurred during Unit 1, recording C/N values in a range between 14 and 10. Atomic H/C ratios ranged between 1.13 and 6.66 with an average value of 1.65. The lowest values were recorded between the bottom of the record and approximately 0.77 m (~ 3.9 cal kyr BP) with ranging values between 1.13 and 2.26 with an average of 1.39. Highest values are depicted from 0.77 m to the top of the record averaging values of 2.62.

The *n*-alkane data obtained from the Padul-15-05 sediments show that shorter carbon chains were abundant during Unit 1. CPI values were higher than 2, averaging values of around 7 and representing an odd over even carbon chain and a good preservation of the organic matter in the sediments, the lowest values, with an average of 2.6, occurred during the Unit 1 around 3.07–2.31 m depth (~ 9.7 to 7.6 cal kyr BP), and the highest values averaging 11.8 occurred between 2.31 and 2.15 m depth (from ~7.5 to 7.2 cal kyr BP). Short-chain abundance shows peaks of higher values at 3.10 m (~9.6 cal kyr BP), 2.55 m (~ 8.5 cal kyr BP), 2.30 m (~ 7.5 cal kyr BP), 1.40 m (~ 5.4 cal kyr BP), from 1.10 to 0.8 m (~ 4.6–4 cal kyr BP), 0.52 m (~ 2.7 cal kyr BP) and from 0.4–0.33 m (~ 1.3–0.8 cal kyr BP). Mid-chain abundance shows the highest values between the bottom and 2.26 m (between ~11.6 and 7.6 cal kyr BP) with an average of approximately 24%, depicting a maximum between 2.90 and 2.31 m (~9.5 to 7.6 cal kyr BP) with average values of around 40%. The lowest values are recorded during the last 1.15 m (~4.7 cal kyr BP). Long-chain abundance shows high values averaging ~ 81% between 2.26 and 1.40 m (~ 7.5 to 5.4 cal kyr BP) and reached maximum values around 0.60 m (~3.2 cal kyr BP) and between 0.45 m (~ 1.9 cal kyr BP), and the last 0.22 cm (~ 0.1 cal kyr BP).

3.3. Pollen and spores

Pollen grains from terrestrial, aquatic species and spores were identified and the taxa higher than around 1% were plotted in the pollen diagrams (Supplementary Figs. S4, S5 and S6). The most representative taxa are plotted in a summary pollen diagram (Fig. 5). In this study, we used the variations between Mediterranean forest taxa, xerophytes, hygrophytes and algae for paleoenvironmental and paleoclimatic variability in the study area. The fluctuations in arboreal pollen (AP, including Mediterranean tree species) have previously been used in other nearby Sierra Nevada records as a proxy for regional humidity changes (Jiménez-Moreno and Anderson, 2012; Ramos-Román et al., 2016). The abundance of the Mediterranean woods (i.e., evergreen and deciduous *Quercus*, *Olea*, *Pistacia*) has been used as a proxy for climate change in many other studies in the western Mediterranean region, with higher forest development generally meaning higher humidity (Fletcher and Sánchez-Goñi, 2008; Fletcher et al., 2013). On the other hand, increases in xerophyte pollen taxa (i.e., *Artemisia*, *Ephedra*, Amaranthaceae), representative of steppe vegetation, have been used as an indication of aridity in this area (Carrión et al., 2007; Anderson et al., 2011). Variability in wetland angiosperms and algae could be indicative of local change in the surrounding vegetation and lake level fluctuations. Singh et al. (1990) suggested that Cyperaceae and *Typha* could be considered swamp- indicative when co-occurring with freshwater algae (*Cosmarium*, Zygnemataceae). Currently, the dominant plant species in the Padul wetland is the common reed, *Phragmites australis*, in fact very common in semi-arid wetlands with shallow water levels (Moro et al., 2004). This species has thrives whenever a wetlands becomes drier (Hudon, 2004). Van Geel et al. (1983) described the occurrences of *Zygnema* and *Mougeotia* as characteristic of shallow lake water environments. The chlorophyceae *Botryococcus* is an indicator of freshwater environments in relatively productive fens, temporary pools, ponds or lakes (Guy-Ohlson, 1992). Clausing (1999) point out that *Botryococcus* abundance is higher in sediment of shallow water lakes and/or littoral environment in deeper lakes. Three pollen zones were visually identified with the help of a cluster analysis using the program CONISS (Grimm, 1987).

The pollen results are described subsequently, distinguishing three

Table 4
Linear r (Pearson) correlation between geochemical proxies and pollen data from the Padul-15-05 record. Statistical treatment was performed using the Past software (http://palaeo-electronica.org/2001_1/past/issue1_01.htm).

	C/N ratio	H/C ratio	TOC	MS	Poaceae	Algae	Hygrophyte	Short-chain	Mid-chain	Long-chain	S	Br	K/Si	Ca	Sr
C/N ratio		5.33E-16	6.30E-33	9.48E-13	9.41E-07	7.14E-02	2.11E-10	3.67E-05	0.0093249	9.69E-01	2.15E-30	1.24E-13	4.56E-08	1.05E-24	5.60E-20
H/C ratio	−0.60595		4.97E-16	1.25E-54	0.24997	0.83873	0.014101	1.36E-11	0.16571	0.040739	4.80E-11	3.45E-08	1.03E-10	9.55E-09	9.85E-17
TOC	0.79396	−0.60645		1.03E-12	8.08E-08	0.00097023	5.41E-10	1.26E-11	0.00011256	0.80183	2.41E-65	1.04E-36	1.02E-10	2.05E-39	6.36E-49
MS	−0.54666	0.90279	−0.54594		0.58699	0.64816	0.018814	2.33E-09	1.03E-01	0.12274	4.44E-09	2.02E-07	2.83E-11	1.60E-06	4.34E-15
Poaceae	0.39277	−0.095815	0.42633	−0.045323		0.00096771	5.25E-07	0.37586	5.61E-01	0.99854	8.46E-08	0.00018098	0.019496	6.83E-06	0.00031762
Algae	−0.14967	−0.016988	−0.27025	−0.038078	−0.27031		0.0028618	0.6669	9.08E-05	0.0073904	0.0043751	8.23E-05	0.00030366	0.13141	0.00039267
Hygrophyte	0.49514	−0.20278	0.4852	−0.19424	0.40108	−0.24514		0.29595	1.53E-08	0.00034311	1.54E-12	5.19E-10	0.016645	1.67E-10	1.44E-06
Short-chain	−0.33565	0.52387	−0.52465	0.4706	−0.074081	0.036044	−0.087385		0.0010611	5.42E-22	6.36E-08	1.93E-08	4.50E-05	8.70E-08	2.48E-11
Mid-chain	0.21524	−0.11572	0.31522	−0.13612	0.048675	−0.31926	0.44853	0.26917		1.93E-48	5.05E-05	3.19E-03	6.52E-02	0.00011163	3.23E-05
Long-chain	0.0032797	−0.17016	0.021023	−0.12875	−0.00015362	0.2216	−0.29331	−0.6921	−0.88146		0.66657	0.66508	5.68E-01	0.7461	0.99199
S	0.77416	−0.51013	0.93201	−0.46179	0.42573	−0.23457	0.54234	−0.43076	0.32998	−0.036081		9.63E-42	3.78E-12	4.77E-34	5.58E-40
Br	0.56396	−0.43716	0.81996	−0.41423	0.30507	−0.32002	0.48565	−0.44574	0.24327	0.036253	0.84907		2.40E-07	8.36E-27	7.26E-26
K/Si	−0.43366	0.50252	−0.50258	0.51532	−0.19316	0.29481	−0.1979	0.33204	−0.15353	−0.047753	−0.53426	−0.41189		0.22728	2.33E-21
Ca	−0.72099	0.45282	−0.83631	0.38503	−0.36269	0.12543	−0.49757	0.42671	−0.31537	0.027119	−0.80209	−0.74218	0.10054		5.65E-19
Sr	0.6649	−0.61781	0.88208	−0.59051	0.2939	−0.28956	0.38657	−0.51813	0.33788	0.00084107	0.83951	0.73296	−0.68263	−0.65119	

major phases during the Holocene:

3.3.1. From ~ 11.6 to 7.6 cal kyr BP (from ~3.67 to 2.31 m)

The early and early middle Holocene, from ~ 11.6 to 7.6 cal kyr BP, is characterized by high abundance of Mediterranean forest, averaging relative percentage values of approximately 58%. The most representative arboreal tree taxon between ~ 11.6 to 9.7 cal kyr BP is evergreen *Quercus,* reaching maximum values of around. 50%. A decrease in the Mediterranean forest and an increase in hygrophytes and Poaceae occurred between 10.1 and 9.6 cal kyr BP (from 3.28 to 3.01 m). Deciduous *Quercus* show increasing trends between 9.5 and 7.6 cal kyr BP (~ 2.91 to 2.31 m), recording average maxima with values of around 22% at that time. Hygrophytes reach maxima average values of approximately 17%, from ~ 9.8 to 8.8 cal kyr BP (from 3.16 to 2.63 m). Algae display a decreasing trend from around 9% (from ~ 11.6 to 9.9 cal kyr BP/3.67 to 3.20 m) to 2% (from ~ 9.9 to 7.6 cal kyr BP/3.20 to 2.34 m). These algawedecline between ~ 11.6 and 9.9 cal kyr BP is due to the lowering of *Zygnema* spores. An increase in the soil mycorrhizal fungus *Glomus* type occurs from ~9.6 to 9.3 cal kyr BP (from 3.01 to 2.80 m).

This transition between the early and middle Holocene is featured by a slight decrease in deciduous *Quercus* and in wetland plants such as Cyperaceae and *Typha* type.

3.3.2. From ~ 7.6 to 4.7 cal kyr BP (from ~ 2.34 to 1.15 m)

The middle Holocene from ~ 7.6 to 4.7 cal kyr BP is still characterized by high values of Mediterranean forest (averaging values of ~ 58%) interrupted by several events of forest decrease. One of the most significant Mediterranean forest declines (up to 26%) parallel hygrophyte and Poaceae rise between ~ 7.5 and 7.3 cal kyr BP (2.28 to 2.21 m). A slight increase in algae also occurred around ~ 7.6 to 7.1 cal kyr BP (2.31 to 2.11 m). A second decrease in the Mediterranean forest occurred at ~ 6 cal kyr BP (from around 1.65 m), also characterized by the increase in hygrophytes to maximum values around 40%, and the increase in *Pinus* of around 5 to 12%. A third remarkable decrease in Mediterranean forest occurred between ~ 5.5 to 5.4 cal kyr BP (around 1.43 to 1.39 m), also characterized by the increase of the aquatic component. These three previous events of decrease in forest decline are accompanied by slight *Glomus* type increases.

3.3.3. From ~ 4.7 cal kyr BP to present (from ~ 1.15 m to top)

The middle to late Holocene transition (~ 4.7 cal kyr BP/~ 1.15 m) is characterized by the decrease in Mediterranean forest, in particular in the deciduous tree taxa, and the increase in *Pinus*, shrubs (i.e., Ericaceae) and xerophytes and Asteraceae (mainly Cichorioideae) (Ramos-Román et al., 2018).

3.4. Spectral analysis

Spectral analysis was performed on the pollen percentage record in order to find cyclical periodicities in the Mediterranean forest from the Padul-15-05 record using REDFIT analysis (Schulz and Mudelsee, 2002) detecting a periodicities of around ~ 2070, 1430 and 1100 yr. Wavelet analyses show significant cycles (p = .05) in the Mediterranean forest taxa time series with periodicities around ~ 2070 and 1100 yr during the early and middle Holocene period and ~ 1430 yr periodicity since ~ 4.7 cal kyr BP to Present (Supplementary Fig. S7).

4. Discussion

4.1. Holocene climate change in Padul and the western Mediterranean region

4.1.1. The earliest Holocene

During the earliest Holocene (~ 11 to 10 cal kyr BP) a transition period from glacial to interglacial conditions occurred in the Padul area

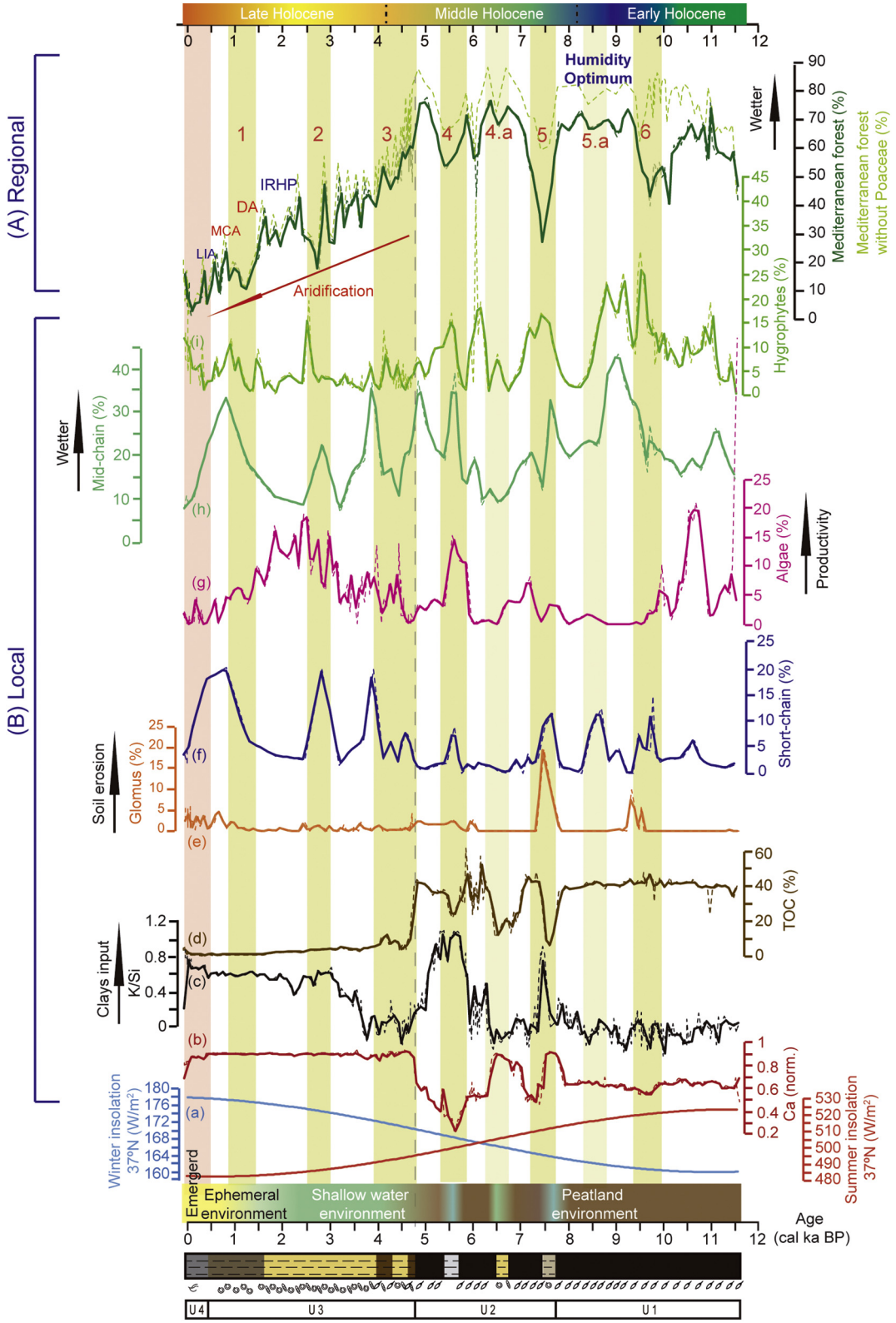

Fig. 6. Padul-15-05 local environment development during the Holocene deduced from a comparison between different pollen, organic and inorganic geochemistry proxies from the Holocene part of the Padul-15-05 record and summer and winter insolation for the Sierra Nevada latitude. A) Regional response determines by Mediterranean forest taxa (%). B) Local response: (a) Summer and winter insolation calculated for 37° N (Laskar et al., 2004), (b) Ca (norm.) (c) K/Si ratio (clays input), (d) Total organic carbon percentage (TOC %), (e) *Glomus* type (%) (f), Short-chain (%), (g) Algae percentage from the pollen analysis (h) Mid-chain (%), (i) Hygrophytes percentage. Beige shadings are showing arid and cold event during the early and middle Holocene determine by the decline in Mediterranean forest component and showing the response in the local environment. Proxies were resampled at 80 yr (in bold) by lineal interpolation using Past software (http://palaeo-electronica.org/2001_1/past/issue1_01.htm). U: Unit.

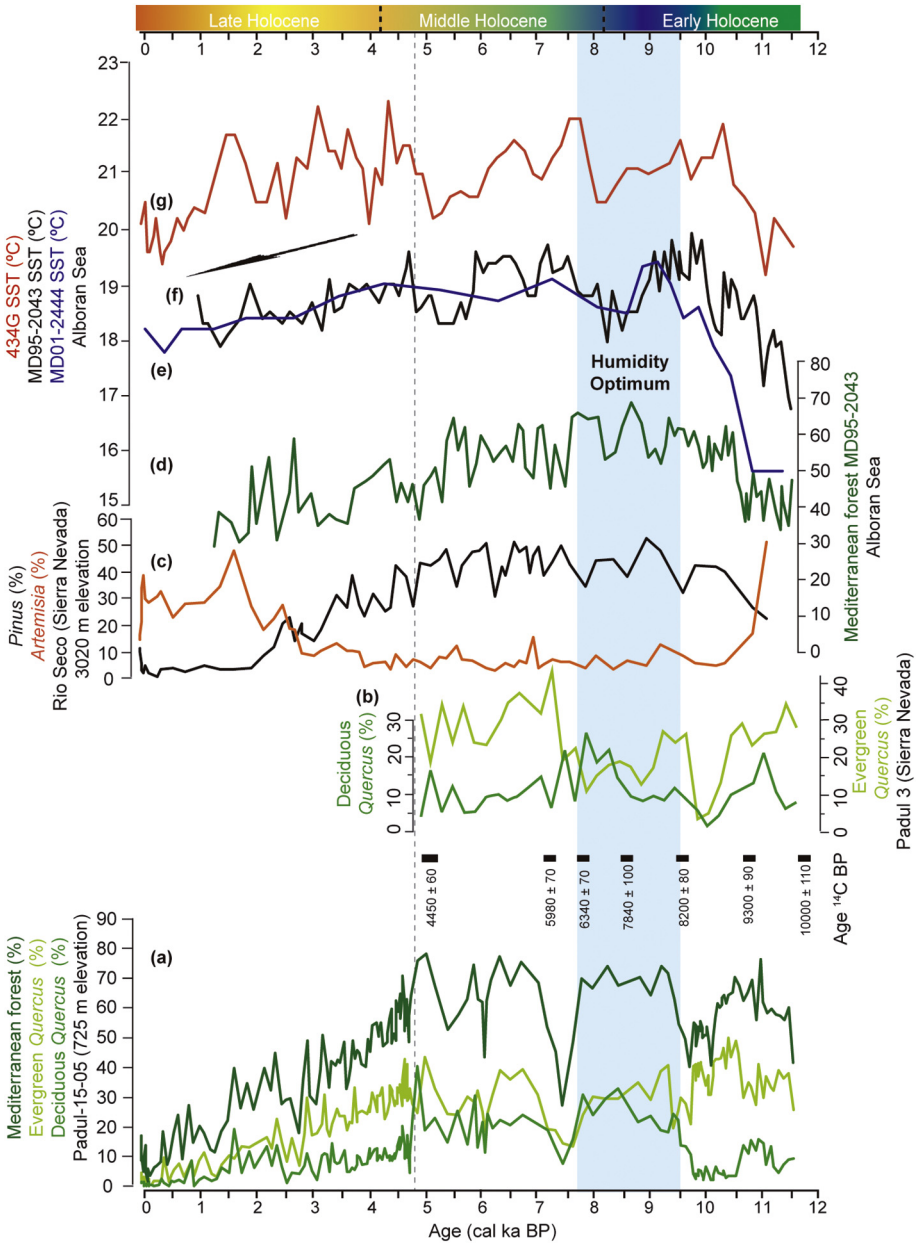

Fig. 7. Comparison for the Holocene between different pollen taxa from the Padul-15-05 record with a previously pollen record in the same area and other pollen and temperature proxies from nearly records in the western Mediterranean region (see records locations in Supplementary Fig. S8). (a) Deciduous *Quercus*, Evergreen *Quercus* and Mediterranean forest percentages in the Padul-15-05 record, (b) Deciduous *Quercus* and Evergreen *Quercus* in a previously record in the Padul peat bog (Pons and Reille, 1988), (c) Percentage of *Pinus* and *Artemisia* in the nearly Laguna de Rio Seco record, Sierra Nevada (Anderson et al., 2011), (d) Temperate and Mediterranean forest percentage for the MD95–2043 record, Alboran Sea (Fletcher and Sánchez-Goñi, 2008), (e) Alkenone sea surface temperature (SST) reconstruction from the MD01–2444, Alboran Sea (Martrat et al., 2004), (f) Alkenone SST reconstruction from the MD95–2043 record, Alboran Sea (Cacho et al., 1999), (g) Alkenone SST reconstruction from the 434G record, Alboran Sea (Rodrigo-Gámiz et al., 2014b). Blue shading represents the humidity optimum during the Holocene in the western Mediterranean region. (For interpretation of the references to colour in this figure legend, the reader is referred to the web version of this article.)

and the pollen assemblages were dominated by evergreen *Quercus* and to a lesser extent, mesic forest species such as deciduous *Quercus*. Local environment proxies show a development of a peatland environment in the Padul basin (organic facies featured by higher values of TOC and C/N and lower values of mid-chain, short-chain and S; Fig. 6), which indicate low water levels at that time. The increase in Mediterranean forest taxa may be interpreted as a regional vegetation response to a climate change to warmer and more humid conditions than earlier on during the cold and dry Younger Dryas, agreeing with the increasing trend in SSTs reconstructions from the Alboran Sea (Cacho et al., 1999; Martrat et al., 2004; Rodrigo-Gámiz et al., 2014b; Fig. 7; Supplementary Fig. S8). The observed peak of evergreen *Quercus* is consistent with previously described glacial-interglacial vegetation transition from Southern Europe indicating that a cold-dry steppe was followed by pre-temperate open woodland [including *Juniperus*, *Pinus*, *Betula*, *Quercus;* van der Hammen et al. (1971)]. These results agree with the previous pollen records from Padul, which also show a widespread evergreen *Quercus* forest after the postglacial epoch (Pons and Reille, 1988) and other high-resolution pollen studies in the western Mediterranean region that show a similar forest change with high abundance of Mediterranean taxa (Fletcher and Sánchez-Goñi, 2008; Fig. 7). These results are also consistent with vegetation variability in the Middle Atlas Mountains of Morocco depicting high values of evergreen *Quercus rotundifolia* at that time (Lamb and van der Kaars, 1995). A forest expansion is also observed in the nearby, but higher elevation site, Laguna de Rio Seco in Sierra Nevada (Supplementary Fig. S8), but in this case, it is mostly due to *Pinus* expansion after a pollen assemblage dominated by steppe vegetation (Anderson et al., 2011; Fig. 7). This dissimilarity is probably explained by the altitudinal difference between the two sites (Padul = 750 m vs. Laguna de Rio Seco = 3000 m), being influenced by different vegetation belts (mesomediterranean vs. oromediterranean belt; see Table 1). The continental pollen record of the cave site Carihuela, inland Granada at the supramediterranean altitude, also shows a clear oak dominance during this period (Carrión et al., 1999; Fernández et al., 2007).

A punctual increase in algae (principally dominated by *Zygnema* type) also occurred within this peat-dominated and shallow water period at around ~ 10.5 cal kyr BP. We suggest that this increase in

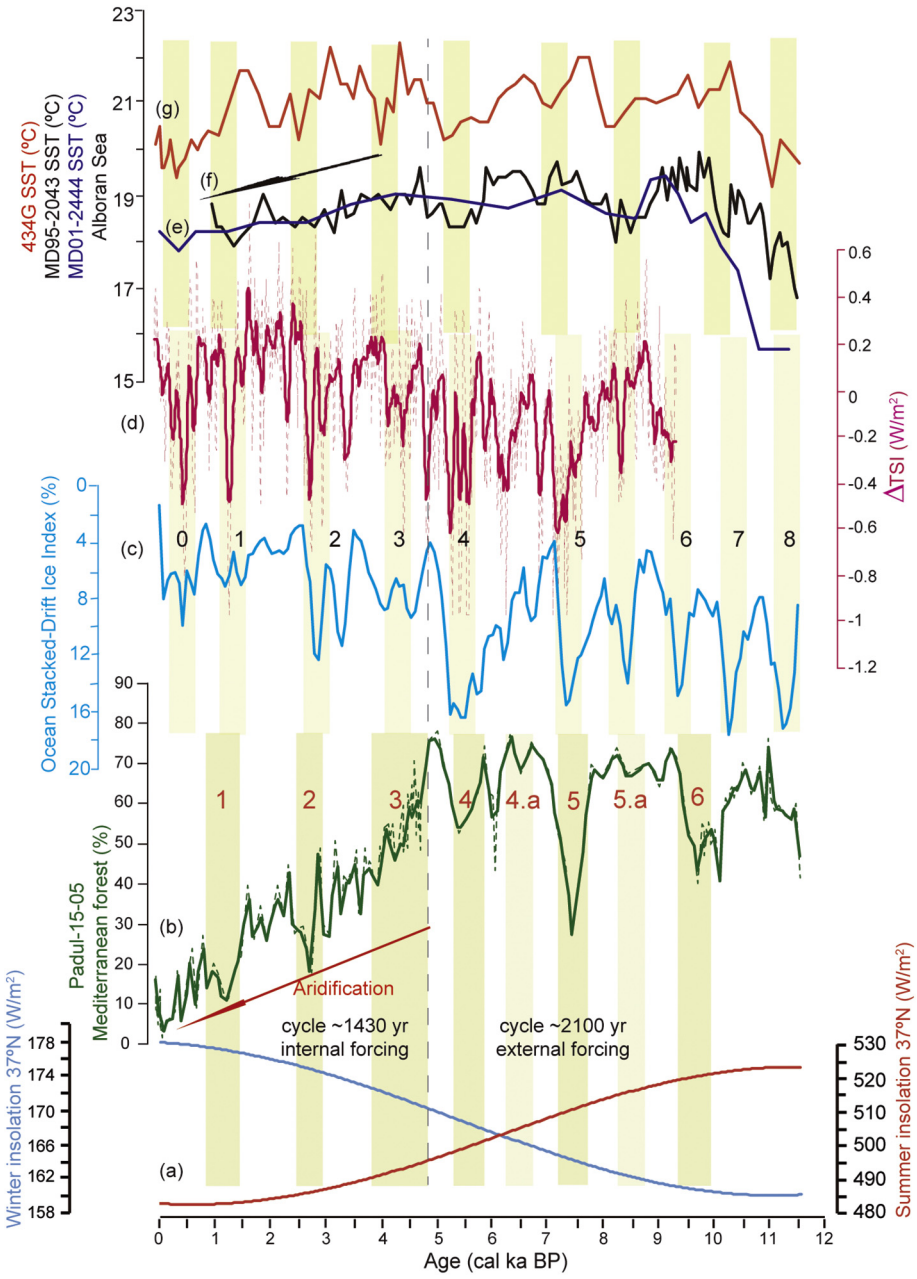

Fig. 8. Holocene climate periodicity from the Padul-15-05 record determine by declines in the Mediterranean forest component and comparison with other North Atlantic records. (a) Summer and winter insolation calculated for 37° N (Laskar et al., 2004), (b) Mediterranean forest taxa (c) Ocean stacked percentage of the Drift Ice Index (reversed) from the North Atlantic (Bond et al., 2001), (d) Total solar irradiance (TSI) anomaly reconstruction from cosmogenic radionuclide from a Greenland ice core (Steinhilber et al., 2009), (e) Alkenone sea surface temperature (SST) reconstruction from the MD01–2444, Alboran Sea (Martrat et al., 2004), (f) Alkenone SST reconstruction from the MD95–2043 record, Alboran Sea (Cacho et al., 1999), (g) Alkenone SST reconstruction from the 434G record, Alboran Sea (Rodrigo-Gámiz et al., 2014b). Beige shadings highlight decreases in Mediterranean forest and coldest events related with decreases in total solar irradiance and decreases in SST. A linear r (Pearson) correlation was calculated between the Mediterranean forest abundances and the TSI anomaly ($r = 0.43$; $p < .001$; between ~ 9.4 and 4.7 cal kyr BP and $r = 0.37$; $p < .001$; between 4.7 cal kyr BP and present). In order to obtain equally spaced time series the Mediterranean forest and the TSI anomaly data were previously resampled at 50 years (linear interpolation), the Mediterranean forest data was detrended (only between 4.7 cal kyr BP to Present) and the TSI anomaly smoothed to a five-point average.

algae could probably be linked with an increase in productivity in the wetland resulting from increased temperatures during a warm pulse recorded in the North Atlantic ice record (Bond et al., 2001; Fig. 8).

4.1.2. Early and middle Holocene and humidity optimum

The early to middle Holocene (from ~ 10 to 4.7 cal kyr BP) in the Padul-15-05 record is featured by the highest values of Mediterranean forest showing the expansion in mesic components (e.g. deciduous *Quercus*), agreeing with the temperate phase of vegetation transition during interglacial periods (described by van der Hammen et al., 1971 and reviewed by Tzedakis, 2007; Supplementary Fig. S9). The local Padul wetland environment within this period (~ 10 to 4.7 cal kyr BP) was characterized by generally low water levels, triggering high occurrence of wetland plants, which accumulated in great amounts, generating peat sedimentation related with higher organic content and/or anoxic/reducing conditions and associated geochemical signals (i.e. higher values of TOC, C/N, S and an increase in mid-chain; Figs. 4 and 6). There is an apparent contradiction between the regional vegetation signal, which indicates high humidity, and local sedimentary proxies, which pointing to low water levels in the area. This contradiction could be explained due to very strong evapotranspiration rates during Holocene summer insolation maxima (Laskar et al., 2004) even if annual (mostly winter) precipitation was the highest (Fig. 6). Low lake levels during the regionally humid early Holocene have also been observed in other records from the southern Mediterranean area, pointing to the same high-evaporative summer insolation phenomenon (Lamb and van der Kaars, 1995; Reed et al., 2001; Magny et al., 2007).

Despite the overall humid conditions interpreted for the early and middle Holocene, millennial-scale climate variability occurred (see Section 4.1.4 below) and wettest conditions are observed between ~ 9.5 to 7.6 cal kyr BP in the Padul-15-05 record. This humidity optimum is indicated regionally by the maximum expansion of mesic forest species (deciduous *Quercus*). Our new results from Padul agree with the previously described Holocene climate evolution in the western Mediterranean region, which also show a wetter early and middle Holocene and a transition to drier conditions during the late Holocene (Fletcher

et al., 2013; Anderson et al., 2011; Carrión et al., 2010 among others). The maximum in humidity occurred during summer insolation maxima and thus during the warmest Holocene conditions shown by paleoclimate records such as the Greenland ice core record temperature reconstruction (Alley, 2000), the decrease in the Drift Ice Index in the north Atlantic records and in total solar irradiance (TSI) and regionally the SST reconstructions in the Alboran Sea (Bond et al., 2001; Cacho et al., 1999; Rodrigo-Gámiz et al., 2014b; Steinhilber et al., 2009; Figs. 7 and 8). Support for the timing of the Holocene humidity optimum recorded in Padul-15-05 comes from a number of paleoclimatic studies from nearby places. For example, previous pollen results from the Padul sedimentary sequence show a similar increase in deciduous *Quercus* and maximum humidity at the same time (Pons and Reille, 1988; Fig. 7). The nearby alpine site of Laguna de Rio Seco in Sierra Nevada indicates that the early and middle Holocene is characterized by more abundant mesic vegetation and the maximum in algae and aquatic plants, indicating that humid maximum occurred prior to ~ 7.8 cal kyr BP (Anderson et al., 2011). Jimenez-Espejo et al. (2008) in a study in the Algero-Balearic basin described that the end of the Holocene, humid conditions occurred between ~ 7.7 and 7.2 cal kyr BP and a synthesis about circum-Mediterranean vegetation change analysis determined that two principal climatic phases occurred during the early and middle Holocene, with a more humid phase from 11 to 7.5 cal kyr BP and a transition phase from 7 to 5.5 cal kyr BP, the later one mostly related to decreasing insolation and the installation of the present climate dynamics (Jalut et al., 2009). Dormoy et al. (2009) also described the maximum in humidity in the Mediterranean region during the early and middle Holocene between 9.5 and 7.5 cal kyr BP, resulting from maximum seasonal anomaly characterized by greatest winter precipitation and minima in precipitation during summer. However, some discrepancies exist about the timing of the mesic maximum within this generally humid period in the Mediterranean region and continental and marine records from southern Iberia and north Africa pointed out that the mesic maximum occurred later on during the middle Holocene (Lamb and van der Kaars, 1995; Carrión, 2002; Fletcher and Sánchez-Goñi, 2008). Supporting our hypothesis, Anderson et al. (2011) suggested that this difference in timing between montane and subalpine forest development and water lake levels could be associated to the different effect that summer insolation maxima and higher seasonality provoked in effective precipitation and water levels during the early Holocene. In lower elevation with higher evaporations rates during summer, compared to higher elevation areas and alpine lakes with lower summer temperatures and higher snowpack during winter and subsequently high lake level.

The early Holocene thermal maximum could be explained by maximum orbital-scale summer insolation (Laskar et al., 2004; Figs. 6 and 8). The early Holocene humidity maximum was likely due to enhanced fall/winter precipitation, consistent with global climate models predicting that summer insolation maxima favor the land/sea temperature contrast in the Mediterranean thus enhancing the winter rainfall (Meijer and Tuenter, 2007).

This occurred at the same time that the Intertropical Convergence Zone was displaced northward (prior to ~ 6 ka) into the Sahara and Arabian deserts (Gasse and Roberts, 2004). However, Arz et al. (2003) and Tzedakis (2007) concluded that summer monsoon did not reach further than the African subtropical desert during the early and middle Holocene and would not have had a direct influence over the northern Mediterranean coast.

Sedimentation at that time in the Padul basin is homogeneous peat but the local proxies show some oscillations (see in Section 4.1.4).

4.1.3. End of the humid period and significant environmental change around 4.7 cal kyr BP

The Padul-15-05 record shows the most significant climatic change affecting both regional and local environment at ~ 4.7 cal kyr BP, right at the middle to late Holocene transition. This paleoenvironmental change is regionally depicted by the beginning of a strong decrease in Mediterranean (especially in the deciduous) forest, indicating progressive climate drying conditions, a slight increase in *Pinus*, and an increase in Ericaceae (Ramos-Román et al., 2018). The significant development of heathlands (Ericaceae) during the middle to late Holocene transition could be indicative of reduced insolation under still a relatively humid climate. This agrees with other studies that show that heathlands increased under increasing precession (decreasing summer insolation), suggesting a thriving response to reduced thermal seasonality (Fletcher and Sánchez-Goñi, 2008). Similar vegetation changes, with the decline in mesic forest species and the increase in shrubs such as Ericaceae, have previously been recorded in other terrestrial and marine pollen archives from the western Mediterranean region during the transition to the late Holocene (e.g., Carrión, 2002; Carrión et al., 2003, 2007; Carrión et al., 2010; Fletcher and Sánchez-Goñi, 2008;) pointing to a regional response to climate aridification and reduction in seasonality (i.e. cooler summers and warmer winters). The timing of this change agrees with Magny et al. (2002) who described the period at 4.5 cal kyr BP, as a crucial transition from wetter to drier climate in the Mediterranean region. In addition, Jalut et al. (2009), described the aridification process in the Mediterranean region since 5.5 cal kyr BP.

This climatic change also locally affected the Padul wetland environment, and sedimentation changed drastically from mostly peat (unit 2) to carbonate-rich clays (unit 3) rich in aquatic organisms (charophytes and gastropods; between ~ 4.7 to 1.5 cal kyr BP; Ramos-Román et al., 2018) pointing to an increase in the lake level. This sedimentary change is principally featured in the geochemistry by a decrease in organic content, a decrease in the aquatic plants in the lake [lower values of TOC (Ramos-Román et al., 2018), C/N and generally decrease in mid-chain abundance], an increase in Ca and in the palynomorph record by a continuously increase in algae (principally dominated by *Botryococcus*; Ramos-Román et al., 2018). In addition, a higher terrestrial and detrital input occurred during the aridification trend, observed in the Padul-15-05 sequence by a slight increasing trend in soil erosion (*Glomus*) and clastic input (higher K/Si), most likely due to the decrease in Mediterranean forest in the area.

As discussed above, there seems to be a contradiction between regional proxies, showing increased aridity, and local proxies showing increasing lake levels. This could be explained due to varied effect of the orbital-scale decrease in summer insolation in both environments. A decrease in summer insolation would trigger a decrease in the sea surface temperature reducing the wind system and precipitation from sea to shore during winter (Marchal et al., 2002) and would also shorten the length of the growing season thus provoking forest depletion. However, decreasing summer insolation would also reduce the seasonality and would lower evapotranspiration during summer, affecting the evaporation/precipitation balance. This along with the continuous groundwater supply in the Padul basin would explain the increasing lake levels in the Padul wetland during the late Holocene (Fig. 6). Some authors also related this aridification trend to the establishment of the current atmospheric dynamics with a northward shift of the westerlies -and as consequence a long-term NAO-like positive mode- affecting the western Mediterranean region (Magny et al., 2012). In addition, this climatic shift coincided with the end of the African Humid Period (5.5 ka; deMenocal et al., 2000). Shanahan et al. (2015) suggested that the decrease in rainfall at this time shown in the African paleoclimate records (tropical and subtropical Africa) is related to declining summer insolation and the gradual southward migration of the tropical monsoon.

A general decreasing trend in SST is recorded in the Alboran Sea since around 4–3 cal kyr BP (Figs. 7 and 8; Cacho et al., 1999; Martrat et al., 2004; Rodrigo-Gámiz et al., 2014b), which supports our hypothesis of a lower sea/land temperature contrast. However, the higher resolution study of Rodrigo-Gámiz et al. (2014b) shows increasing SST superimposed between the generally decreasing trend, coinciding with wetter periods such as for example the end of the Iberian-Roman Humid

Period.

Within the context of regional progressive aridification, the late Holocene (sensu *lato*) from Padul could mainly be divided into two phases, a first phase from ~ 4.7 to 3 cal kyr BP characterized by the slight increasing trend in *Botryococcus* and the declining trend in mid-chain abundance, and a second phase from ~ 3 to 1.5 cal kyr BP featured by maximum values in *Botryococcus* and a minimum in mid-chain abundance (Fig. 6). Relative maxima in Mediterranean forest between ~ 2.6 and 1.6 cal kyr BP, indicating regional humidity, co-occurred with the maximum in *Botryococcus* algae also indicating either high relative lake level and/or more productivity in the lake (Ramos-Román et al., 2018). High relative humidity in this region is supported by the fact that this mild climatic event occurred during the well-known Iberian Roman Humid Period (IRHP) between 2.6 and 1.6 cal kyr BP (Martín-Puertas et al., 2009).

The aridification trend enhanced around ~ 1.5 cal kyr BP and culminated with a further environmental change to an ephemeral lake (even emerged during the last centuries). This is deduced by the remarkable increase in detritic sedimentation (K/Si; Fig. 6), probably due to higher soil erosion (increase in *Glomus* type) partially enhanced by human activities in the surroundings of the lake since this time (Ramos-Román et al., 2018), and by a continuous increase in mid-chain, short-chain abundance and wetland plants while *Botryococcus* and other aquatic organisms (especially charophytes) declined. Aquatic plants probably expanded in the Padul wetland area when the water levels dropped. This increasing trend in mid-chain and short-chain abundances started to decline during the last centuries when the wetland became emerged and higher human impact occurred (for more information about human activities see Ramos-Román et al., 2018).

The ~ 4.7 to Present natural aridification process was interrupted by millennial-scale climate variability with several especially arid events occurring around ~ 4.7–4, 2.7 and 1.3 cal kyr BP (see next section; 4.1.4).

4.1.4. Millennial-scale Holocene climate variability

In addition to the long-term trends observed in the Padul paleoenvironments, likely driven by insolation-related climate changes during the Holocene, the high-resolution multi-proxy record from Padul-15-05 record shows millennial-scale vegetation, lake level and sedimentary oscillations that can be related with global climate variability and cooling events detected in North Atlantic archives. In this respect, the Padul-15-05 sequence shows arid-cooling climatic events around ~ 9.6, 8.5, 7.5, 6.5, 5.4, 4.7–4, 2.7 and 1.3 cal kyr BP, generally identified in both regional (decreases in the Mediterranean forest suggesting regional cooling and aridity) and local proxies (increases in clays input, short-chain, mid-chain and hygrophyte) and with periodicities of about 2100 and 1100 years. These short-scale climatic changes affected sedimentation and local lake level in the Padul environment, generally with increases in carbonate (charophytes and gastropods) and clastic sedimentation, hygrophytes, short-chain and mid-chain abundances pointing to higher lake levels probably triggered by cooling and less evaporation in the wetland, enhanced erosion due to deforestation and increase in plants adapted to more aquatic wetland environments (Fig. 6). Some of these events are manifested in the Padul-15-05 record clearly in both regional and local proxies (~ 9.6, 7.5, 5.4, 4.7–4, 2.7, 1.3 cal kyr BP) but some others are more evident in the local signal (for example events at 8.5 and 6.5 cal kyr BP). The two latter ones probably indicating that those events were less severe and/or problems recording them sufficiently well in the pollen. During the last ~ 4.7 cal kyr BP, during the establishment of the modern climatic dynamics and the decrease in summer insolation, a shallow lake formed and these cold events are also associated with declines in the lake productivity (for example, reductions in algae before and after the IRHP; Fig. 6).

Most of these climatic events have been described in other Mediterranean paleoclimate records, considering the radiocarbon age uncertainties between the different studies. For example, Jalut et al. (2000) also described aridification phases for the western Mediterranean region around ~10.9–9.7, 8.4–7.6 and 5.3–4.2, 4.3–3.4, 2.8–1.7 and 1.3–0.75 cal kyr BP, showing that these events were correlated with glacial advances, ^{14}C anomalies, North Atlantic records and paleohydrological changes in European mid-latitudes suggesting that they were a regional response to global climate change. Some arid events around ~ 9.6–9.5, 8.4–8 and 6–5.5 cal kyr BP, have been also identified as arid and cool events in a study from the eastern and western Mediterranean region (Dormoy et al., 2009). Fletcher and Zielhofer (2013) detected this rapid climate changes relating these arid periods with high-latitude cooling events around 6–5 and 3.5–2.5 cal kyr BP. Recently, Zielhofer et al. (2017) show a decrease in western Mediterranean winter rain at 11.4, 10.3, 9.2, 8.2, 7.2, 6.6, 6.0, 5.4, 5.0, 4.4, 3.5, 2.9, 2.2, 1.9, 1.7, 1.5, 1.0, 0.7, and 0.2 cal kyr BP. They associated these events during the early Holocene with Atlantic coolings probably related with meltwater discharges and weakening of the Atlantic overturning circulation. In contrast, after ~ 5 cal kyr BP, they related these Atlantic cooling episodes to humid winters and negative NAO conditions evidencing a change in the ocean-atmospheric system in response to the external forcing. In the nearby Sierra Nevada, arid events are detected around 3.8–3.1 and 1.8–0.7 cal kyr BP (Laguna de la Mula; Jiménez-Moreno et al., 2013). Cold and arid events detected in the Padul-15-05 record at ~ 9.6, 8.5, 7.5, 6.5, 5.4, 4.7–4, 2.7 and 1.3 cal kyr BP have been also identified in North Atlantic records (Bond events 6, 5, 4, 3, 2, 1; Bond et al., 2001; Fig. 8), which indicate that these events were recorded at hemispheric scales. The good correspondence with the timing of these cold events with decreases in solar activity recorded by the TSI anomaly during the Holocene could show a link between them (Steinhilber et al., 2009; Fig. 8). The correlation between the Mediterranean forest from Padul and TSI anomaly ($r = 0.43$; $p < .001$ between ~ 9.4 to 4.7 cal kyr BP and $r = 0.37$; $p < .001$ between 4.7 cal kyr BP to present) seems to show that a link exists between solar and environmental variability in the Mediterranean area. This would agree with previous studies showing a sun-climate-environment relationship (Zielhofer et al., 2017). However, we are still far to understanding how solar activity affects climate and deeper studies are necessary in order to provide with information about the behavior between solar, climate and environmental relationships and the link between the Mediterranean and North Atlantic regions.

4.1.5. Forcing mechanisms of Holocene millennial-scale climate variability in the western Mediterranean region

The time series analysis done on the Mediterranean forest (regional proxy) from the Padul-15-05 record using wavelet analysis shows millennial-scale cyclical periodicities during the early, middle and late Holocene. This analysis helps to understand the relationship between the regional paleoenvironmental periodicity in the proxy data from the Padul record and external (i.e. solar activity) and internal (oceanic-atmospheric dynamics) forcings during the Holocene in the western Mediterranean. Cyclicities of around ~ 2100 yr and ~ 1100 yr are detected in the Mediterranean forest taxa time series with a statistically strong cyclical pattern during the early and middle Holocene (the ~ 1100 yr cycle is absent in the late Holocene), and a predominant ~ 1430 yr cycle between the transition of the middle-late Holocene and during the late Holocene (Supplementary Fig. S7). This later cycle could be carefully linked to human impact, which could have altered the natural climatic signal and is recorded in this area since the last ~ 1500 yr (Ramos-Román et al., 2018).

Our results are consistent with similar cyclical patterns detected throughout the North Atlantic records and related with solar activity also describing ~ 2500 and 1000 yr periodicities during the early Holocene (Debret et al., 2007, 2009). A similar periodicity of about 2300 yr is recognized in the $\Delta^{14}C$ residual series from the Greenland Ice Sheet record (Mayewski et al., 1997). This periodicity has also been evidenced in sea surface temperatures (SST) reconstructions in the Aegean Sea in the NE Mediterranean related with glacier advance and

suggesting a solar modulation (Rohling et al., 2002). The ~ 1000 yr periodicity is also stablished as a signal of solar activity in many other records in the Mediterranean and the North Atlantic region (e.g. Debret et al., 2007; Debret et al., 2009 and references therein). Previous cyclostratigraphic analysis performed in the nearby Sierra Nevada alpine area also described cyclical climatic fluctuations with periodicities around 2200 yr (Jiménez-Espejo et al., 2014). In contrast, other spectral analyses carried out in other records in the North Atlantic and western Mediterranean region detected a periodicity of around ~ 1500 yr (e.g. Bond et al., 2001; Rodrigo-Gámiz et al., 2014a). This ~ 1500 yr cycle is also common in other Sierra Nevada records (Jiménez-Espejo et al., 2014; García-Alix et al., 2017) and was interpreted as a solar and atmospheric-oceanic forcing mechanism. In addition, a cycle of ~ 800–760 yr has also been detected in the detailed studied of the late Holocene part of the Padul-15-05 record (Ramos-Román et al., 2018) and in other records in the Sierra Nevada (Ramos-Román et al., 2016). This cycle could be related to the second harmonic of the ~ 1600–1500 yr cycle. These results show very mixed interpretations with both solar and/or oceanic forcing mechanisms being described to explain cyclicities in the different proxies. Debret et al. (2009) in a non-stationary time series analysis tried to differentiate the different forcing mechanisms for the different cyclicities and also described an intensification of the ~ 1600 yr period detected in the North Atlantic area (terrestrial and marine records and interpreted of both solar and oceanic origin) in the last 5000 years. Those authors then interpret this cyclical periodicity change as a shift in dynamics from mostly external (solar) forcing to mostly internal (oceanic) forcing.

According to this, the results from the Padul-15-05 Holocene record suggest that the regional climate variability during the early and middle Holocene was partially due to external forcing (i.e. solar irradiance) and variability during the late Holocene (since ~ 4.7 cal kyr BP) was dominated by the effect of internal forcing (atmospheric-oceanic dynamic) -established since the NAO system influencing the western Mediterranean region- enhanced since ~ 5 cal kyr BP (Debret et al., 2007, 2009). Fletcher et al. (2013) described a shift in the millennial-scale periodicity since around ~ 6 cal kyr BP related with the establishment of the actual climate system in the western Mediterranean region. The similarities between the millennial-scale oscillations observed in the Padul-15-05 record with the total solar irradiance anomaly (TSI) and cooling events in the North Atlantic region (e.g. Bond et al., 2001; Steinhilber et al., 2009; Fig. 8) support the solar-atmospheric-oceanic link in the Atlantic-western Mediterranean region previously suggested (Debret et al., 2009).

5. Conclusions

Variations in regional and local paleoenvironmental and paleoclimate proxies from the Padul-15-05 Holocene record helped to interpret climate and paleoenvironmental change during the last 11,600 years in southern Iberia and the western Mediterranean region. The comparison of our record with other regional and global oceanic-atmospheric-terrestrial studies aided to comprehend the origin of these paleoenvironmental changes.

The early and middle Holocene was characterized by overall humid and warm conditions and a humidity optimum between ~ 9.5 and 7.6 cal kyr BP, humid winters and very hot and dry summers and a higher seasonality, occurred in this area due to summer insolation maxima. These interpretations come from the highest occurrence of deciduous tree species and humid conditions in the local environment (higher mid-chain abundance) in the Padul-15-05 core. Summer insolation maxima translated into very high evaporation rates and lowest lake level conditions triggering the abundance of wetland plants and the deposition of peat related with the higher TOC. A transition phase towards drier conditions is recorded in the middle Holocene between ~ 7.6 and 4.7 cal kyr BP through a decrease in deciduous forest and a higher water level variability mainly associated with variations in Ca, S, K/Si ratio and TOC content. This environmental change was probably due to a reduction in seasonality and decreasing summer insolation, which also locally triggered less evaporation and the alternation of water level increase within a peatland environment. This climate transition culminated in the Padul area with a significant environmental change at ~ 4.7 cal kyr BP, featured by a regional aridification trend that produced a decreasing trend in the Mediterranean forest. Precipitation decreased in the late Holocene but the decrease in summer insolation locally triggered less evaporation and the development of a shallow water lake environment and a significant sedimentary change characterized by higher values of Ca an increasing trend in clay minerals (K/Si ratio), and the decrease in TOC. The Padul shallow lake environment became ephemeral since ~ 1.5 cal kyr BP and even emerged during the last centuries probably induced by human impact.

The Padul-15-05 record also shows millennial-scale climate variability with declines in Mediterranean forest showing cool-arid events and variability in the lake level around 9.6, 8.5, 7.5, 6.5, 5.4, 4.7–4, 3, 2.7 and 1.3 cal kyr BP, associated with cold events in the North Atlantic records. According to the regional (Mediterranean forest taxa) paleoclimate results from the non-stationary time-series analyses, climate during the early and middle Holocene could have been influenced by external solar forcing with typical periodicities around 1100 and 2100 yrs., and the last ~ 4700 years could have been associated with an internal oceanic/atmospheric control (also in part related with solar forcing) as periodicities changed towards ~ 1430 yr in the regional paleoclimate proxy. However, this later periodicity has to be taken carefully as human impact is evident in the area during the last 1500 yr, probably altering somehow the climatic record.

We would like to emphasise on the importance of carrying out multi-proxy analyses containing both regional and local signals and a non-stationary time-series analysis in order to clarify the links between terrestrial-oceanic-atmospheric connections in Holocene paleoclimatic studies.

Acknowledgments

This work was supported by the project P11-RNM-7332 funded by Consejería de Economía, Innovación, Ciencia y Empleo de la Junta de Andalucía, the project (CGL2013-47038-R) funded by Ministerio de Economía y Competitividad of Spain and fondo Europeo de desarrollo regional FEDER and the research group RNM0190 (Junta de Andalucía). M. J. R.-R. acknowledges the predoctoral and postdoctoral funding provided by Consejería de Economía, Innovación, Ciencia y Empleo de la Junta de Andalucía (P11-RNM-7332). J.C. acknowledges the PhD funding provided by Ministerio de Economía y Competitividad (CGL2013-47038-R). J.S.C. acknowledges the support of projects CGL-BOS-2012-34717, CGL-BOS 2015-68604, and Fundación Séneca 19434/PI/14. A.G.-A. was also supported by a Ramón y Cajal Fellowship RYC-2015-18966 of the Spanish Government (Ministerio de Economía y Competividad). Javier Jaimez (CIC-UGR) is thanked for graciously helping with the coring, the drilling equipment and logistics. We would also like to thank to two anonymous reviewers and the editor (Fabienne Marret-Davies) for their valuable suggestions.

Appendix A. Supplementary data

Supplementary data to this article can be found online at https://doi.org/10.1016/j.gloplacha.2018.06.003.

References

Alpert, P., Baldi, M., Ilani, R., Krichak, S., Price, C., Rodó, X., Saaroni, H., Ziv, B., Kishcha, P., Barkan, J., Mariotti, A., Xoplaki, E., 2006. Chapter 2 relations between climate variability in the Mediterranean region and the tropics: ENSO, south Asian and African monsoons, hurricanes and Saharan dust. Developments in Earth and Environmental Sciences 4, 149–177. http://dx.doi.org/10.1016/S1571-9197(06)80005-4.

Anderson, R.S., Jiménez-Moreno, G., Carrión, J.S., Pérez-Martínez, C., 2011. Postglacial history of alpine vegetation, fire, and climate from Laguna de Río Seco, Sierra Nevada, southern Spain. Quat. Sci. Rev. 30, 1615–1629. http://dx.doi.org/10.1016/j.quascirev.2011.03.005.

Arz, H.W., Lamy, F., Pätzold, J., Müller, P.J., Prins, M., 2003. Mediterranean moisture source for an early-Holocene humid period in the northern Red Sea. Science 300, 118. http://dx.doi.org/10.1126/science.1080325.

Bar-Matthews, M., Ayalon, A., Gilmour, M., Matthews, A., Hawkesworth, C.J., 2003. Sea–land oxygen isotopic relationships from planktonic foraminifera and speleothems in the eastern Mediterranean region and their implication for paleorainfall during interglacial intervals. Geochim. Cosmochim. Acta 67, 3181–3199. http://dx.doi.org/10.1016/S0016-7037(02)01031-1.

Beug, H.-J., 2004. Leitfaden der Pollenbestimmung für Mitteleuropa und angrenzende Gebiete, Fisch. Stuttg., Leitfaden der Pollenbestimmung für Mitteleuropa und angrenzende Gebiete, Friedrich Pfeil, München. pp. 61.

Bond, G., Kromer, B., Beer, J., Muscheler, R., Evans, M.N., Showers, W., Hoffmann, S., Lotti-Bond, R., Hajdas, I., Bonani, G., 2001. Persistent solar influence on North Atlantic climate during the Holocene. Science 294, 2130. http://dx.doi.org/10.1126/science.1065680.

Bush, R.T., McInerney, F.A., 2013. Leaf wax n-alkane distributions in and across modern plants: Implications for paleoecology and chemotaxonomy. Geochim. Cosmochim. Acta 117, 161–179. http://dx.doi.org/10.1016/j.gca.2013.04.016.

Cacho, I., Grimalt, J.O., Pelejero, C., Canals, M., Sierro, F.J., Flores, J.A., Shackleton, N., 1999. Dansgaard-Oeschger and Heinrich event imprints in Alboran Sea paleotemperatures. Paleoceanography 14, 698–705. http://dx.doi.org/10.1029/1999PA900044.

Cacho, I., Grimalt, J.O., Canals, M., Sbaffi, L., Shackleton, N.J., Schönfeld, J., Zahn, R., 2001. Variability of the western Mediterranean Sea surface temperature during the last 25,000 years and its connection with the northern hemisphere climatic changes. Paleoceanography 16, 40–52. http://dx.doi.org/10.1029/2000PA000502.

Carrión, J.S., 2002. Patterns and processes of late quaternary environmental change in a montane region of southwestern Europe. Quat. Sci. Rev. 21, 2047–2066. http://dx.doi.org/10.1016/S0277-3791(02)00010-0.

Carrión, J.S., Munuera, M., Navarro, C., Burjachs, F., Dupré, M., Walker, M.J., 1999. The palaeoecoloical potential of pollen records in caves: the case of Mediterranean Spain. Quat. Sci. Rev. 18, 1061–1073. http://dx.doi.org/10.1016/S0277-3791(98)00002-X.

Carrión, J.S., Sánchez-Gómez, P., Mota, J.F., Yll, R., Chaín, C., 2003. Holocene vegetation dynamics, fire and grazing in the sierra de Gádor, southern Spain. The Holocene 13, 839–849. http://dx.doi.org/10.1191/0959683603hl662rp.

Carrión, J.S., Fuentes, N., González-Sampériz, P., Quirante, L.S., Finlayson, J.C., Fernández, S., Andrade, A., 2007. Holocene environmental change in a montane region of southern Europe with a long history of human settlement. Quat. Sci. Rev. 26, 1455–1475. http://dx.doi.org/10.1016/j.quascirev.2007.03.013.

Carrión, J.S., Fernández, S., González-Sampériz, P., Gil-Romera, G., Badal, E., Carrión-Marco, Y., López-Merino, L., López-Sáez, J.A., Fierro, E., Burjachs, F., 2010. Expected trends and surprises in the Lateglacial and Holocene vegetation history of the Iberian Peninsula and Balearic Islands. Review of Palaeobotany and Palynology 162, 458–475. http://dx.doi.org/10.1016/j.revpalbo.2009.12.007.

Castillo Martín, A., Benavente Herrera, J., Fernández Rubio, R., Pulido Bosch, A., 1984. Evolución y ámbito hidrogeológico de la laguna de Padul (Granada). In: Las Zonas Húmedas en Andalucía. Monografías de DGMA-MOPU.

Chapman, S.J., 2001. Sulphur forms in open and afforested areas of two Scottish peatlands. Water Air Soil Pollut. 128, 23–39. http://dx.doi.org/10.1023/A:1010365924019.

Cheddadi, R., Yu, G., Guiot, J., Harrison, S.P., Prentice, I.C., 1997. The climate of Europe 6000 years ago. Clim. Dyn. 13, 1–9. http://dx.doi.org/10.1007/s003820050148.

Clausing, A., 1999. Palaeoenvironmental significance of the green alga Botryococcus in the lacustrine rotliegend (upper carboniferous - lower permian). Hist. Biol. 13, 221–234. http://dx.doi.org/10.1080/08912969909386582.

Combourieu-Nebout, N., Peyron, O., Dormoy, I., Desprat, S., Beaudouin, C., Kotthoff, U., Marret, F., 2009. Rapid climatic variability in the West Mediterranean during the last 25 000 years from high resolution pollen data. Clim. Past 5, 503–521. http://dx.doi.org/10.5194/cp-5-503-2009.

Cranwell, P.A., 1984. Lipid geochemistry of sediments from Upton broad, a small productive lake. Org. Geochem. 7, 25–37. http://dx.doi.org/10.1016/0146-6380(84)90134-7.

Cranwell, P., Eglinton, G., Robinson, N., 1987. Lipids of aquatic organisms as potential contributors to lacustrine sediments—II. Org. Geochem. 11, 513–527.

Davis, J.C., Sampson, R.J., 1986. Statistics and Data Analysis in Geology. Wiley, New York.

Debret, M., Bout-Roumazeilles, V., Grousset, F., Desmet, M., McManus, J.F., Massei, N., Sebag, D., Petit, J.-R., Copard, Y., Trentesaux, A., 2007. The origin of the 1500-year climate cycles in Holocene North-Atlantic records. Clim. Past 3, 569–575. http://dx.doi.org/10.5194/cp-3-569-2007.

Debret, M., Sebag, D., Crosta, X., Massei, N., Petit, J.-R., Chapron, E., Bout-Roumazeilles, V., 2009. Evidence from wavelet analysis for a mid-Holocene transition in global climate forcing. Quat. Sci. Rev. 28, 2675–2688. http://dx.doi.org/10.1016/j.quascirev.2009.06.005.

Demenocal, P., Ortiz, J., Guilderson, T., Sarnthein, M., 2000. Coherent high- and low-latitude climate variability during the Holocene warm period. Science 288, 2198–2202. http://dx.doi.org/10.1126/science.288.5474.2198.

Dormoy, I., Peyron, O., Combourieu Nebout, N., Goring, S., Kotthoff, U., Magny, M., Pross, J., 2009. Terrestrial climate variability and seasonality changes in the Mediterranean region between 15 000 and 4000 years BP deduced from marine pollen records. Clim. Past 5, 615–632. http://dx.doi.org/10.5194/cp-5-615-2009.

El Aallali, A., Nieto, J.M.L., Raya, F.A.P., Mesa, J.M., 1998. Estudio de la vegetación forestal en la vertiente sur de Sierra Nevada (Alpujarra Alta granadina). Itinera Geobot. 11, 387–402.

Faegri, K., Iversen, J., 1989. Textbook of Pollen Analysis. Wiley, New York.

Feijtel, T.C., Salingar, Y., Hordijk, C.A., Sweerts, J.P.R.A., Van Breemen, N., Cappenberg, T.E., 1989. Sulfur cycling in a dutch moorland pool under elevated atmospheric S-deposition. Water Air Soil Pollut. 44, 215–234. http://dx.doi.org/10.1007/BF00279256.

Fernández, S., Fuentes, N., Carrión, J.S., González-Sampériz, P., Montoya, E., Gil, G., Vega-Toscano, G., Riquelme, J.A., 2007. The Holocene and upper Pleistocene pollen sequence of Carihuela cave, southern Spain. Geobios 40, 75–90. http://dx.doi.org/10.1016/j.geobios.2006.01.004.

Ficken, K.J., Li, B., Swain, D., Eglinton, G., 2000. An n-alkane proxy for the sedimentary input of submerged/floating freshwater aquatic macrophytes. Org. Geochem. 31, 745–749.

Fletcher, W.J., Sánchez-Goñi, M.F., 2008. Orbital- and sub-orbital-scale climate impacts on vegetation of the western Mediterranean basin over the last 48,000 yr. Quat. Res. 70, 451–464. http://dx.doi.org/10.1016/j.yqres.2008.07.002.

Fletcher, W.J., Zielhofer, C., 2013. Fragility of Western Mediterranean landscapes during Holocene rapid climate changes. In: Long-term Degradation of Fragile Landscape Systems. 103. pp. 16–29. http://dx.doi.org/10.1016/j.catena.2011.05.001.

Fletcher, W.J., Debret, M., Goñi, M.F.S., 2013. Mid-Holocene emergence of a low-frequency millennial oscillation in western Mediterranean climate: implications for past dynamics of the North Atlantic atmospheric westerlies. The Holocene 23, 153–166. http://dx.doi.org/10.1177/0959683612460783.

Florschütz, F., Amor, J.M., Wijmstra, T.A., 1971. Palynology of a thick quaternary succession in southern Spain. Palaeogeography, Palaeoclimatology, Palaeoecology 10, 233–264. http://dx.doi.org/10.1016/0031-0182(71)90049-6.

García-Alix, A., Delgado Huertas, A., Martín Suárez, E., 2012. Unravelling the Late Pleistocene habitat of the southernmost woolly mammoths in Europe. Quat. Sci. Rev. 32, 75–85. http://dx.doi.org/10.1016/j.quascirev.2011.11.007.

García-Alix, A., Jiménez-Espejo, F.J., Toney, J.L., Jiménez-Moreno, G., Ramos-Román, M.J., Anderson, R.S., Ruano, P., Queralt, I., Delgado Huertas, A., Kuroda, J., 2017. Alpine bogs of southern Spain show human-induced environmental change superimposed on long-term natural variations. Sci. Rep. 7, 7439. http://dx.doi.org/10.1038/s41598-017-07854-w.

Gasse, F., Roberts, C.N., 2004. Late quaternary hydrologic changes in the arid and semiarid belt of Northern Africa. In: Diaz, H.F., Bradley, R.S. (Eds.), The Hadley Circulation: Present, Past and Future. Springer Netherlands, Dordrecht, pp. 313–345. http://dx.doi.org/10.1007/978-1-4020-2944-8_12.

Gelpi, E., Schneider, H., Mann, J., Oró, J., 1970. Hydrocarbons of geochemical significance in microscopic algae. Phytochemistry 9, 603–612. http://dx.doi.org/10.1016/S0031-9422(00)85700-3.

Grimm, E.C., 1987. CONISS: a Fortran 77 program for stratigraphically constrained cluster analysis by the method of incremental sum of squares. Comput. Geosci. 13, 13–35.

Guy-Ohlson, D., 1992. Botryococcus as an aid in the interpretation of palaeoenvironment and depositional processes. Review of Palaeobotany and Palynology 71, 1–15. http://dx.doi.org/10.1016/0034-6667(92)90155-A.

Hammer, O., Harper, D.A.T., Ryan, P.D., 2001. PAST: paleontological statistics software package for education and data analysis. Palaeontol. Electron. 4 (1), 9.

Hudon, C., 2004. Shift in wetland plant composition and biomass following low-level episodes in the St. Lawrence River: looking into the future. Canadian Journal of Fisheries and Aquatic Sciences 61, 603–617. http://dx.doi.org/10.1139/f04-031.

Huntley, B., Prentice, I.C., 1988. July temperatures in Europe from pollen data, 6000 years before present. Science 241, 687–690. http://dx.doi.org/10.1126/science.2414866.687.

Hurrell, J.W., 1995. Decadal trends in the North Atlantic oscillation: regional temperatures and precipitation. Science 269, 676. http://dx.doi.org/10.1126/science.2695224.676.

Jalut, G., Esteban Amat, A., Bonnet, L., Gauquelin, T., Fontugne, M., 2000. Holocene climatic changes in the western Mediterranean, from south-east France to south-East Spain. Palaeogeogr. Palaeoclimatol. Palaeoecol. 160, 255–290. http://dx.doi.org/10.1016/S0031-0182(00)00075-4.

Jalut, G., Dedoubat, J.J., Fontugne, M., Otto, T., 2009. Holocene circum-Mediterranean vegetation changes: climate forcing and human impact. Quat. Int. 200, 4–18. http://dx.doi.org/10.1016/j.quaint.2008.03.012.

Jimenez-Espejo, F.J., Martinez-Ruiz, F., Rogerson, M., González-Donoso, J.M., Romero, O.E., Linares, D., Sakamoto, T., Gallego-Torres, D., Rueda Ruiz, J.L., Ortega-Huertas, M., Perez Claros, J.A., 2008. Detrital input, productivity fluctuations, and water mass circulation in the westernmost Mediterranean Sea since the Last Glacial Maximum. Geochemistry, Geophysics, Geosystems 9 n/a-n/a. https://doi.org/10.1029/2008GC002096.

Jiménez-Espejo, F.J., García-Alix, A., Jiménez-Moreno, G., Rodrigo-Gámiz, M., Anderson, R.S., Rodríguez-Tovar, F.J., Martínez-Ruiz, F., Giralt, S., Delgado Huertas, A., Pardo-Igúzquiza, E., 2014. Saharan aeolian input and effective humidity variations over western Europe during the Holocene from a high altitude record. Chem. Geol. 374–375, 1–12. http://dx.doi.org/10.1016/j.chemgeo.2014.03.001.

Jiménez-Moreno, G., Anderson, R.S., 2012. Holocene vegetation and climate change recorded in alpine bog sediments from the Borreguiles de la Virgen, Sierra Nevada, southern Spain. Quat. Res. 77, 44–53. http://dx.doi.org/10.1016/j.yqres.2011.09.006.

Jiménez-Moreno, G., García-Alix, A., Hernández-Corbalán, M.D., Anderson, R.S., Delgado-Huertas, A., 2013. Vegetation, fire, climate and human disturbance history in the southwestern Mediterranean area during the late Holocene. Quat. Res. 79, 110–122. http://dx.doi.org/10.1016/j.yqres.2012.11.008.

Johnsen, S.J., Clausen, H.B., Dansgaard, W., Fuhrer, K., Gundestrup, N., Hammer, C.U.,

Iversen, P., Jouzel, J., Stauffer, B., Steffensen, J.P., 1992. Irregular glacial interstadials recorded in a new Greenland ice core. Nature 359, 311–313. http://dx.doi.org/10.1038/359311a0.
Kalugin, I., Daryin, A., Smolyaninova, L., Andreev, A., Diekmann, B., Khlystov, O., 2007. 800-yr-long records of annual air temperature and precipitation over southern Siberia inferred from Teletskoye Lake sediments. Quat. Res. 67, 400–410. http://dx.doi.org/10.1016/j.yqres.2007.01.007.
Lamb, H.F., van der Kaars, S., 1995. Vegetational response to Holocene climatic change: pollen and palaeolimnological data from the middle atlas, Morocco. The Holocene 5, 400–408. http://dx.doi.org/10.1177/095968369500500402.
Laskar, J., Robutel, P., Joutel, F., Gastineau, M., Correia, A.C.M., Levrard, B., 2004. A long-term numerical solution for the insolation quantities of the Earth. Astron. Astrophys. 428, 261–285. http://dx.doi.org/10.1051/0004-6361:20041335.
Lionello, P., Malanotte-Rizzoli, P., Boscolo, R., 2006. Mediterranean climate variability. Elsevier.
López-Buendía, A.M., Whateley, M.K.G., Bastida, J., Urquiola, M.M., 2007. Origins of mineral matter in peat marsh and peat bog deposits, Spain. Int. J. Coal Geol. 71, 246–262.
Magny, M., de Beaulieu, J.-L., Drescher-Schneider, R., Vannière, B., Walter-Simonnet, A.-V., Miras, Y., Millet, L., Bossuet, G., Peyron, O., Brugiapaglia, E., Leroux, A., 2007. Holocene climate changes in the central Mediterranean as recorded by lake-level fluctuations at Lake Accesa (Tuscany, Italy). Quaternary Science Reviews 26, 1736–1758. http://dx.doi.org/10.1016/j.quascirev.2007.04.014.
Magny, M., Miramont, C., Sivan, O., 2002. Assessment of the impact of climate and anthropogenic factors on Holocene Mediterranean vegetation in Europe on the basis of palaeohydrological records. Palaeogeogr. Palaeoclimatol. Palaeoecol. 186, 47–59. http://dx.doi.org/10.1016/S0031-0182(02)00442-X.
Magny, M., Peyron, O., Sadori, L., Ortu, E., Zanchetta, G., Vannière, B., Tinner, W., 2012. Contrasting patterns of precipitation seasonality during the Holocene in the south- and north-central Mediterranean. J. Quat. Sci. 27, 290–296. http://dx.doi.org/10.1002/jqs.1543.
Marchal, O., Cacho, I., Stocker, T.F., Grimalt, J.O., Calvo, E., Martrat, B., Shackleton, N., Vautravers, M., Cortijo, E., Van Kreveld, S., Andersson, C., Koç, N., Chapman, M., Sbaffi, L., Duplessy, J.-C., Sarnthein, M., Turon, J.-L., Duprat, J., Jansen, E., 2002. Apparent long-term cooling of the sea surface in the northeast Atlantic and Mediterranean during the Holocene. Quat. Sci. Rev. 21, 455–483. http://dx.doi.org/10.1016/S0277-3791(01)00105-6.
Martín-Puertas, C., Valero-Garcés, B.L., Mata, M.P., González-Sampériz, P., Bao, R., Moreno, A., Stefanova, V., 2008. Arid and humid phases in southern Spain during the last 4000 years: the Zoñar Lake record, Córdoba. The Holocene 18, 907–921. http://dx.doi.org/10.1177/0959683608093533.
Martín-Puertas, C., Valero-Garcés, B.L., Brauer, A., Mata, M.P., Delgado-Huertas, A., Dulski, P., 2009. The Iberian-roman humid period (2600-1600 cal yr BP) in the Zoñar Lake varve record (Andalucía, southern Spain). Quat. Res. 71, 108–120. http://dx.doi.org/10.1016/j.yqres.2008.10.004.
Martrat, B., Grimalt, J.O., López-Martínez, C., Cacho, I., Sierro, F.J., Flores, J.A., Zahn, R., Canals, M., Curtis, J.H., Hodell, D.A., 2004. Abrupt temperature changes in the western Mediterranean over the past 250000 years. Science 306, 1762. 10.1126%2Fscience.1101706.
Mayewski, P.A., Meeker, L.D., Twickler, M.S., Whitlow, S., Yang, Q., Lyons, W.B., Prentice, M., 1997. Major features and forcing of high-latitude northern hemisphere atmospheric circulation using a 110,000-year-long glaciochemical series. Journal of Geophysical Research: Oceans 102, 26345–26366. http://dx.doi.org/10.1029/96JC03365.
Mayewski, P.A., Rohling, E.E., Stager, J.C., Karlén, W., Maasch, K.A., Meeker, L.D., Meyerson, E.A., Gasse, F., van Kreveld, S., Holmgren, K., Lee-Thorp, J., Rosqvist, G., Rack, F., Staubwasser, M., Schneider, R.R., Steig, E.J., 2004. Holocene climate variability. Quat. Res. 62, 243–255. http://dx.doi.org/10.1016/j.yqres.2004.07.001.
Meijer, P.T., Tuenter, E., 2007. The effect of precession-induced changes in the Mediterranean freshwater budget on circulation at shallow and intermediate depth. J. Mar. Syst. 68, 349–365. http://dx.doi.org/10.1016/j.jmarsys.2007.01.006.
Meyers, P.A., 1994. Preservation of elemental and isotopic source identification of sedimentary organic matter. Chem. Geol. 114, 289–302. http://dx.doi.org/10.1016/0009-2541(94)90059-0.
Meyers, P.A., Lallier-Vergès, E., 1999. Lacustrine sedimentary organic matter records of late quaternary paleoclimates. J. Paleolimnol. 21, 345–372. http://dx.doi.org/10.1023/A:1008073732192.
Moreno, A., Cacho, I., Canals, M., Grimalt, J.O., Sánchez-Goñi, M.F., Shackleton, N., Sierro, F.J., 2005. Links between marine and atmospheric processes oscillating on a millennial time-scale. A multi-proxy study of the last 50,000 yr from the Alboran Sea (Western Mediterranean Sea). Quat. Sci. Rev. 24, 1623–1636. http://dx.doi.org/10.1016/j.quascirev.2004.06.018.
Moreno, A., López-Merino, L., Leira, M., Marco-Barba, J., González-Sampériz, P., Valero-Garcés, B.L., López-Sáez, J.A., Santos, L., Mata, P., Ito, E., 2011. Revealing the last 13,500 years of environmental history from the multiproxy record of a mountain lake (Lago Enol, northern Iberian Peninsula). J. Paleolimnol. 46, 327–349. http://dx.doi.org/10.1007/s10933-009-9387-7.
Moro, M.J., Domingo, F., López, G., 2004. Seasonal transpiration pattern of Phragmites australis in a wetland of semi-arid Spain. Hydrol. Process. 18, 213–227. http://dx.doi.org/10.1002/hyp.1371.
Ogura, K., Machihara, T., Takada, H., 1990. Diagenesis of biomarkers in Biwa Lake sediments over 1 million years. Org. Geochem. 16, 805–813.
Ortiz, J.E., Torres, T., Delgado, A., Julià, R., Lucini, M., Llamas, F.J., Reyes, E., Soler, V., Valle, M., 2004. The palaeoenvironmental and palaeohydrological evolution of Padul Peat Bog (Granada, Spain) over one million years, from elemental, isotopic and molecular organic geochemical proxies. Org. Geochem. 35, 1243–1260. http://dx.doi.org/10.1016/j.orggeochem.2004.05.013.
Ortiz, J.E., Torres, T., Delgado, A., Llamas, J.F., Soler, V., Valle, M., Julià, R., Moreno, L., Díaz-Bautista, A., 2010. Palaeoenvironmental changes in the Padul Basin (Granada, Spain) over the last 1Ma based on the biomarker content. Palaeogeogr. Palaeoclimatol. Palaeoecol. 298, 286–299. http://dx.doi.org/10.1016/j.palaeo.2010.10.003.
Pérez Raya, F., López Nieto, J., 1991. Vegetación acuática y helofítica de la depresión de Padul (Granada). Acta Bot. Malacitana 16, 373–389.
Peyron, O., Magny, M., Goring, S., Joannin, S., de Beaulieu, J.-L., Brugiapaglia, E., Sadori, L., Garfi, G., Kouli, K., Ioakim, C., Combourieu-Nebout, N., 2013. Contrasting patterns of climatic changes during the Holocene across the Italian peninsula reconstructed from pollen data. Clim. Past 9, 1233–1252. http://dx.doi.org/10.5194/cp-9-1233-2013.
Pons, A., Reille, M., 1988. The holocene- and upper pleistocene pollen record from Padul (Granada, Spain): A new study. Palaeogeography, Palaeoclimatology, Palaeoecology 66, 243–263. http://dx.doi.org/10.1016/0031-0182(88)90202-7.
Ramos-Román, M.J., Jiménez-Moreno, G., Anderson, R.S., García-Alix, A., Toney, J.L., Jiménez-Espejo, F.J., Carrión, J.S., 2016. Centennial-scale vegetation and North Atlantic oscillation changes during the late Holocene in the southern Iberia. Quat. Sci. Rev. 143, 84–95. http://dx.doi.org/10.1016/j.quascirev.2016.05.007.
Ramos-Román, M.J., Jiménez-Moreno, G., Camuera, J., García-Alix, A., Anderson, R.S., Jiménez-Espejo, F.J., Carrión, J.S., 2018. Holocene climate aridification trend and human impact interrupted by millennial- and centennial-scale climate fluctuations from a new sedimentary record from Padul (Sierra Nevada, southern Iberian peninsula). Clim. Past 14 (1), 117–137 10.5194%2Fcp-14-117-2018.
Reed, J.M., Stevenson, A.C., Juggins, S., 2001. A multi-proxy record of Holocene climatic change in southwestern Spain: the Laguna de Medina, Cádiz. The Holocene 11, 707–719. http://dx.doi.org/10.1191/09596830195735.
Reimer, P.J., Bard, E., Bayliss, A., Beck, J.W., Blackwell, P.G., Ramsey, C.B., Buck, C.E., Cheng, H., Edwards, R.L., Friedrich, M., Grootes, P.M., Guilderson, T.P., Haflidason, H., Hajdas, I., Hatté, C., Heaton, T.J., Hoffmann, D.L., Hogg, A.G., Hughen, K.A., Kaiser, K.F., Kromer, B., Manning, S.W., Niu, M., Reimer, R.W., Richards, D.A., Scott, E.M., Southon, J.R., Staff, R.A., Turney, C.S.M., van der Plicht, J., 2013. IntCal13 and Marine13 radiocarbon age calibration curves 0–50,000 years cal BP. Radiocarbon 55, 1869–1887. http://dx.doi.org/10.2458/azu_js_rc.55.16947.
Riera, S., Wansard, G., Julià, R., 2004. 2000-year environmental history of a karstic lake in the Mediterranean pre-Pyrenees: the Estanya lakes (Spain). Catena 55, 293–324. http://dx.doi.org/10.1016/S0341-8162(03)00107-3.
Roberts, N., Brayshaw, D., Kuzucuoğlu, C., Perez, R., Sadori, L., 2011. The mid- Holocene climatic transition in the Mediterranean: Causes and consequences. The Holocene 21, 3–13. http://dx.doi.org/10.1177/0959683610388058.
Rodrigo-Gámiz, M., Martínez-Ruiz, F., Rodríguez-Tovar, F.J., Jiménez-Espejo, F.J., Pardo-Igúzquiza, E., 2014a. Millennial- to centennial-scale climate periodicities and forcing mechanisms in the westernmost Mediterranean for the past 20,000 yr. Quat. Res. 81, 78–93. http://dx.doi.org/10.1016/j.yqres.2013.10.009.
Rodrigo-Gámiz, M., Martínez-Ruiz, F., Rampen, S.W., Schouten, S., Sinninghe Damsté, J.S., 2014b. Sea surface temperature variations in the western Mediterranean Sea over the last 20 kyr: a dual-organic proxy (UK'37 and LDI) approach. Paleoceanography 29, 87–98. http://dx.doi.org/10.1002/2013PA002466.
Rohling, E., Mayewski, P., Abu-Zied, R., Casford, J., Hayes, A., 2002. Holocene atmosphere-ocean interactions: records from Greenland and the Aegean Sea. Clim. Dyn. 18, 587–593. http://dx.doi.org/10.1007/s00382-001-0194-8.
Sachse, D., Radke, J., Gleixner, G., 2006. δD values of individual n-alkanes from terrestrial plants along a climatic gradient – implications for the sedimentary biomarker record. Org. Geochem. 37, 469–483. http://dx.doi.org/10.1016/j.orggeochem.2005.12.003.
Sanz De Galdeano, C., El Hamdouni, R., Chacón, J., 1998. Neotectónica de la fosa del Padul y del Valle de Lecrín. In: Itinerarios Geomorfológicos por Andalucía Oriental. Publicacions de la Universitat de Barcelona, Barcelona, pp. 65–81.
Schulz, M., Mudelsee, M., 2002. REDFIT: estimating red-noise spectra directly from unevenly spaced paleoclimatic time series. Comput. Geosci. 28, 421–426. http://dx.doi.org/10.1016/S0098-3004(01)00044-9.
Shanahan, T.M., McKay, N.P., Hughen, K.A., Overpeck, J.T., Otto-Bliesner, B., Heil, C.W., King, J., Scholz, C.A., Peck, J., 2015. The time-transgressive termination of the African humid period. Nat. Geosci. 8, 140.
Singh, G., Wasson, R.J., Agrawal, D.P., 1990. Vegetational and seasonal climatic changes since the last full glacial in the Thar Desert, northwestern India. In: The Proceedings of the 7th International Palynological Congress (Part I). vol. 64. pp. 351–358. http://dx.doi.org/10.1016/0034-6667(90)90151-8.
Snowball, I., Sandgren, P., 2001. Application of mineral magnetic techniques to paleolimno-logy. Developments in Paleoenvironmental research. Track-ing Environmental Change Using Lake Sediments 2, 217–237.
Steinhilber, F., Beer, J., Fröhlich, C., 2009. Total solar irradiance during the Holocene. Geophys. Res. Lett. 36, 19. http://dx.doi.org/10.1029/2009GL040142.
Talbot, M., 1988. The origins of lacustrine oil source rocks: evidence from the lakes of tropical Africa. Geol. Soc. Lond., Spec. Publ. 40, 29–43.
Talbot, M.R., Livingstone, D.A., 1989. Hydrogen index and carbon isotopes of lacustrine organic matter as lake level indicators. The Phanerozoic Record of Lacustrine Basins and Their Environmental 70, 121–137. http://dx.doi.org/10.1016/0031-0182(89)90084-9.
Torrence, C., Compo, G.P., 1998. A practical guide to wavelet analysis. Bull. Am. Meteorol. Soc. 79, 61–78. http://dx.doi.org/10.1175/1520-0477(1998)079<0061:APGTWA>2.0.CO;2.
Tzedakis, P., 2007. Seven ambiguities in the Mediterranean palaeoenvironmental narrative. Quat. Sci. Rev. 26, 2042–2066.
Valle, F., 2003. Mapa de series de vegetación de Andalucía 1: 400 000. Editorial Rueda,

Madrid.
Valle Tendero, F., 2004. Modelos de Restauración Forestal: Datos botánicos aplicados a la gestión del Medio Natural Andaluz II: Series de vegetación. Consejería de Medio Ambiente de la Junta de Andalucía, Sevilla.
van der Hammen, T., Wijmstra, T.A., Zagwijn, H., 1971. The floral record of the Late Cenozoic of Europe. In: Turekian, K.K. (Ed.), The Late Cenozoic Glacial Ages. Yale University Press, New Haven, pp. 391–424.
van Geel, B., Hallewas, D.P., Pals, J.P., 1983. A late holocene deposit under the Westfriese Zeedijk near Enkhuizen (Prov. of Noord-Holland, The Netherlands): Palaeoecological and archaeological aspects. Review of Palaeobotany and Palynology 38, 269–335. http://dx.doi.org/10.1016/0034-6667(83)90026-X.
Villegas Molina, F., 1967. Laguna de Padul: Evolución geológico-histórica. Estudios Geográficos 28, 561.
Walker, M.J., Berkelhammer, M., Björck, S., Cwynar, L.C., Fisher, D.A., Long, A.J., Lowe, J.J., Newnham, R.M., Rasmussen, S.O., Weiss, H., 2012. Formal subdivision of the Holocene series/epoch: a discussion paper by a working group of INTIMATE (integration of ice-core, marine and terrestrial records) and the subcommission on quaternary stratigraphy (international commission on stratigraphy). J. Quaternary Sci. 27, 649–659. http://dx.doi.org/10.1002/jqs.2565.
Wieder, R.K., Lang, G.E., 1988. Cycling of inorganic and organic sulfur in peat from Big Run Bog, West Virginia. Biogeochemistry 5, 221–242. http://dx.doi.org/10.1007/BF02180229.
Ziegler, M., Jilbert, T., de Lange, G.J., Lourens, L.J., Reichart, G., 2008. Bromine counts from XRF scanning as an estimate of the marine organic carbon content of sediment cores. Geochem. Geophys. Geosyst. 9.
Zielhofer, C., Fletcher, W.J., Mischke, S., De Batist, M., Campbell, J.F.E., Joannin, S., Tjallingii, R., El Hamouti, N., Junginger, A., Stele, A., Bussmann, J., Schneider, B., Lauer, T., Spitzer, K., Strupler, M., Brachert, T., Mikdad, A., 2017. Atlantic forcing of western Mediterranean winter rain minima during the last 12,000 years. Quat. Sci. Rev. 157, 29–51. http://dx.doi.org/10.1016/j.quascirev.2016.11.037.